Ore Geology Reviews 182 (2025) 106581

Contents lists available at ScienceDirect

Ore Geology Reviews

journal homepage: www.elsevier.com/locate/oregeorev

Simple graphical tools to understand the relationship between porphyry composition, hydrothermal alteration, mineralogy and copper-gold grades in porphyry copper deposits

Ross R. Large

CODES, Earth Sciences, University of Tasmania, Tasmania 7005, Australia

ARTICLE INFO

Keywords:
Porphyry copper deposits
Diorite porphyry
PCD alteration plot
Albitisation
Lithogeochemistry
Peschanka
Kharmagtai

ABSTRACT

Alteration zonation in porphyry copper deposits is a standard tool to establish spatial relationships with respect to the best Cu-grade core of the magmatic-hydrothermal system. With the development in recent times of low cost and good quality whole-rock multi-element ICP-MS analysis, large databases of drill hole litho-geochemistry have become available from drilling campaigns of porphyry copper targets. Here I propose some simple graphical tools that use multi-element datasets to evaluate alteration type and their relationship to Cu grades. I suggest a five part methodology; 1) determine the original least altered porphyry composition(s) by using the AI vs CCPI plot, 2) use the molar K/Al vs Na/Al plot to discriminate the basic alteration type, 3) check for alunite and anhydrite using the Ca-Fe-S plot, 4) follow-up with the porphyry copper alteration plot [K/(K + Ca) vs K/(K + Al)] to finalise the discrimination of alteration type. 5) plot all data with Cu > 0.5 % on the K/(K + Ca) vs K/(K + Al) diagram (4 above), as a density plot, to evaluate the relationship between Cu grades and alteration type.

Three case studies are provided that outline the methodology and show the importance of the composition(s) of the host porphyry intrusion(s) in controlling the relationship between Cu-grades, bulk mineralogy and alteration type. Based on these case studies it is clear that not all, or even most, of the samples with greater than 0.5% Cu are always concentrated in the potassic alteration type.

Application of the MINSQ computer program has enabled mineral concentrations to be estimated and plotted on the alteration type diagram K/(K + Ca) vs K/(K + Al) in each of the case studies. This approach suggests that in monzonite and granodiorite based porphyries, K-feldspar replacement of plagioclase subsequently overprinted by white-mica is the key process in the Cu core of the porphyry deposit, whereas in diorite-based porphyries, albitisation of plagioclase is suggested as the dominant alteration process, producing a Cu-Au- bearing sodic-calcic core with little, or only minor, K-feldspar alteration.

1. Introduction

Alteration zonation in VMS and porphyry copper deposits has been used as a practical vectoring tool to determine position in the system relative to economically important mineralized zones within ore deposits since the 1960's (Lowell and Gilbert, 1970; Guilbert and Park, 1986; Singer et al., 2008; Cook et al., 2000; Sangster, 1972; Large, 1977; Franklin et al., 1981; Ohmoto, 1996; Dilles and Singer, 1998; Sillitoe, 2010; Gifkins et al., 2005). VMS systems commonly have a footwall alteration pipe with concentric zonation from the centre to extremities of siliceous to chloritic +/- carbonate to sericitic to K-feldspar-bearing in the distal least-altered volcanics. Hangingwall alteration is commonly weaker, more diffuse, poorly zoned and may include minor albite, chlorite and fuchsite.

Several models of hydrothermal alteration around porphyry copper deposits have been developed over the past 55 years. The initial models, based on the south-west USA porphyries (Lowell and Gilbert, 1970), showed concentric zoning around the central causative porphyry of potassic alteration (K-feldspar, biotite) in the core followed by phyllic (sericite, pyrite) alteration merging outwards to propylitic (chlorite, epidote, albite) alteration at the periphery (Fig. 1a). The model showed a Cu shell overlapping the boundary between the potassic core and sericitic envelope. More recent models (e.g., Sillitoe, 2010), show similar concentric zonation, but with the sericitic alteration above and impinging into the potassic core and sodic-calcic alteration lateral and below the core. Advanced argillic alteration is recognised as a later

E-mail address: Rosslarge2@gmail.com.

https://doi.org/10.1016/j.oregeorev.2025.106581
Received 17 January 2025; Received in revised form 18 March 2025; Accepted 23 March 2025
Available online 9 April 2025

overprint that penetrates downwards over the previous hydrothermal zones (Fig. 1b) (Sillitoe, 2010; Hedenquist et al., 2020).

Early alteration studies employed the petrological microscope to study alteration assemblages (e.g.,Creasey, 1959; Lowell and Gilbert 1970, Gustafson & Hunt, 1975; Eastoe et al., 1987), and more recent work uses various approaches including whole-rock geochemistry, X-ray diffraction, Short Wave-length Infrared (SWIR), mineral chemistry and core scanner technologies (Halley et al, 2020; Pour and Hashim, 2011; Zhou et al., 2022; Cooke et al., 2014; 2020; Wilkinson et al., 2015; Ahmed, 2019; Pacey et al., 2020; Rodrigues and Esterle, 2016; Sorrentino et al., 2024). This contribution focusses on major element whole-rock geochemistry, which has become cost effective and in common use by many exploration companies due to developments in rapid multielement 4-acid digession ICP-MS analysis.

Creasey (1959) was the first to classify alteration in porphyry copper deposits using major element geochemistry into potassic, argillic and propylitic type. I have used the term alteration type rather than alteration zone or field because this study does not include spatial information.

This study to use geochemistry to classify alteration was stimulated by the fact that alteration mapping in the field and especially visual logging alteration in chips and powders from reverse circulation and air-core drilling programs is very difficult, particularly for a geologist with little experience in the porphyry copper environment. Thus, an easy to use and fairly rapid approach employing either well calibrated field pXRF units or 4-acid ICP multielement geochemistry was considered necessary to help train the exploration geologist in the critical process of alteration mapping. This method has been applied most effectively at one of two stages in an exploration program. Either at the start, when only a few holes have been drilled and a rapid appraisal of porphyry alteration types is required to plan future drilling, or secondly at the end of the program when petrology, visual logging and SWIR data are available for integration with assay geochemistry into the process of developing a 3D alteration-mineralisation model for the deposit.

2. Background

In 2001 a simple graphical method for the study of alteration in VMS deposits, called the Alteration Box Plot was published (Large et al., 2001) based on drill hole multi-element geochemistry. This approach relates whole rock geochemistry to alteration mineralogy (Fig. 2) by defining alteration trends from least altered volcanics to more altered based on mineralogy and relatable to proximity to mineralisation. Alteration indexes, such as the Ishikawa alteration index (AI) and the chlorite-carbonate-pyrite index (CCPI), outlined in Fig. 2, were used to measure the intensity of and degree of hydrothermal alteration proximal to the massive sulfide orebodies. The Ishikawa Alteration index is a measure of the replacement of plagioclase and matrix volcanic glass by white mica and chlorite which results in a loss of Na and Ca and gain of K, Fe and Mg. The CCP index measures the gains in Fe and Mg in the altered rock due to the formation of alteration minerals chlorite, Fe-Mg bearing carbonate and pyrite. Weakly altered sericitized volcanics plot toward the right- hand side of the diagram, whereas strongly altered chloritic and pyritic volcanics plot toward the right-hand top corner.

We demonstrated that the alteration box plot is a powerful means of understanding the relationship between mineralogy, lithogeochemistry, and intensity of alteration in zoned alteration systems related to VMS deposits. This method is now in common use by explorers and academics exploring and studying VMS deposits (e.g., Theart et al., 2011; Bachmann et al., 2013; Sharma, 2014; Mills et al., 2016; Gisbert et al., 2021; Siriskha et al., 2019; Gifkins et al 2005; McNulty et al., 2023; Pinto et al., 2021; Krushnisky et al., 2023).

Due to the success of the AI – CCPI plot for studying alteration in VMS systems I have embarked on developing a similar plot for alteration associated with porphyry Cu systems. However, from the beginning I realised this would not be a straight forward task.

The primary issue is that alteration associated with porphyry copper deposits is commonly fracture controlled, rather than pervasive, as is normally the case in VMS alteration. In the core of the porphyry deposit high fluid pressures mean that the intensity of veining and alteration commonly results in the rock being both veined and pervasively altered, but towards the outer alteration zones with lower fluid pressure and infiltration, the veining and intensity of alteration is considerably less and relatively unaltered rock can persist between the veins (Cathles and Shannon, 2007). Titley (1982) proposed three alteration styles to account for this situation a) vein-veinlet alteration, b) selectively pervasive

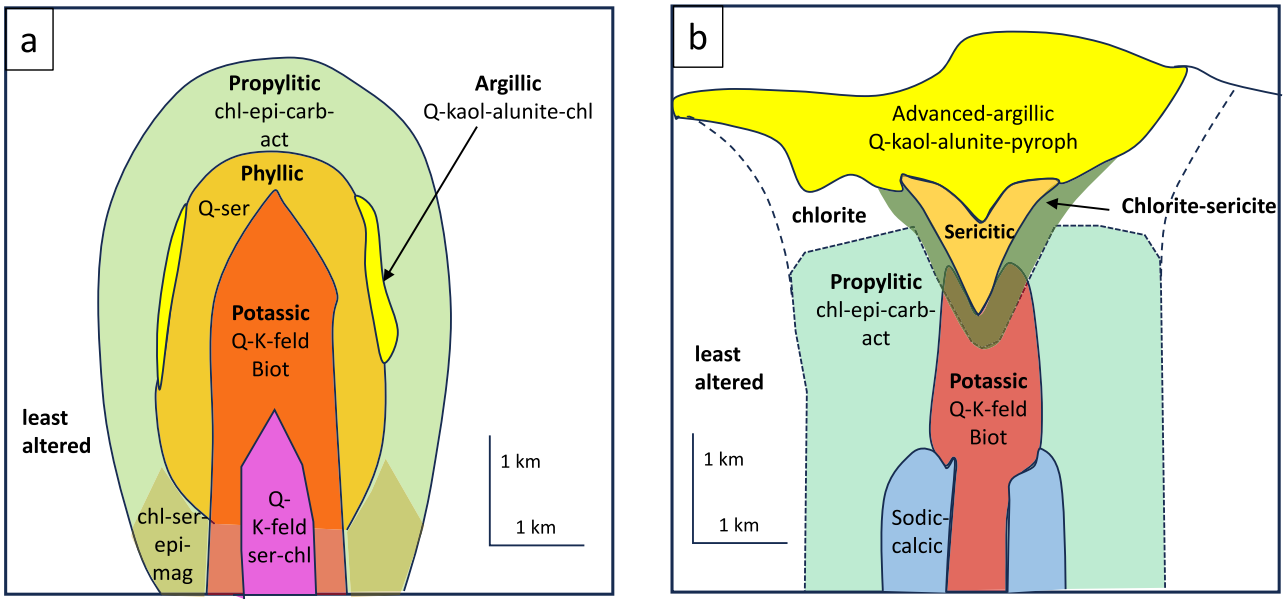

Fig. 1. Two models for porphyry copper alteration patterns: A: South-West USA porphyry alteration model from Lowell and Gilbert (1970); B: general porphyry Cu model adapted from Sillitoe (2010). Abreviations; chl – chlorite, epi-epidote, carb-carbonate, act-actinolite, Q – quartz, kaol- kaolinite, K-feld-K-feldspar, biot-biotite, mag-magnetite, ser-sericite.

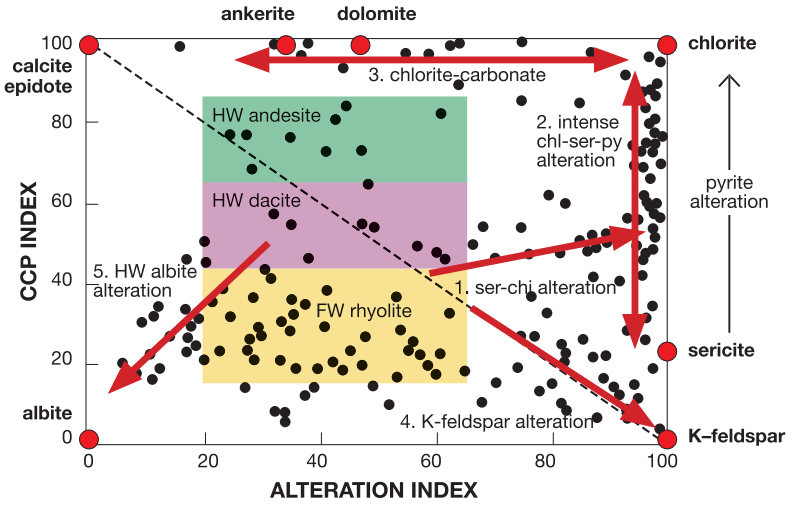

Chlorite-carbonate-pyrite Index (CCPI)

$$CCPI = \frac{100\,(MgO + FeO)}{(MgO + FeO + Na_2O + K_2O)}$$

Ishikawa Alteration Index (AI)

$$AI = \frac{100\,(K_2O + MgO)}{(K_2O + MgO + Na_2O + CaO)}$$

Fig. 2. Alteration trends on the alteration box plot of AI vs CCPI for the Thalanga VHMS deposit (from Large et al., 2001). Abreviations; chl-chlorite, ser-sericite, py-pyrite, HW-hanging wall.

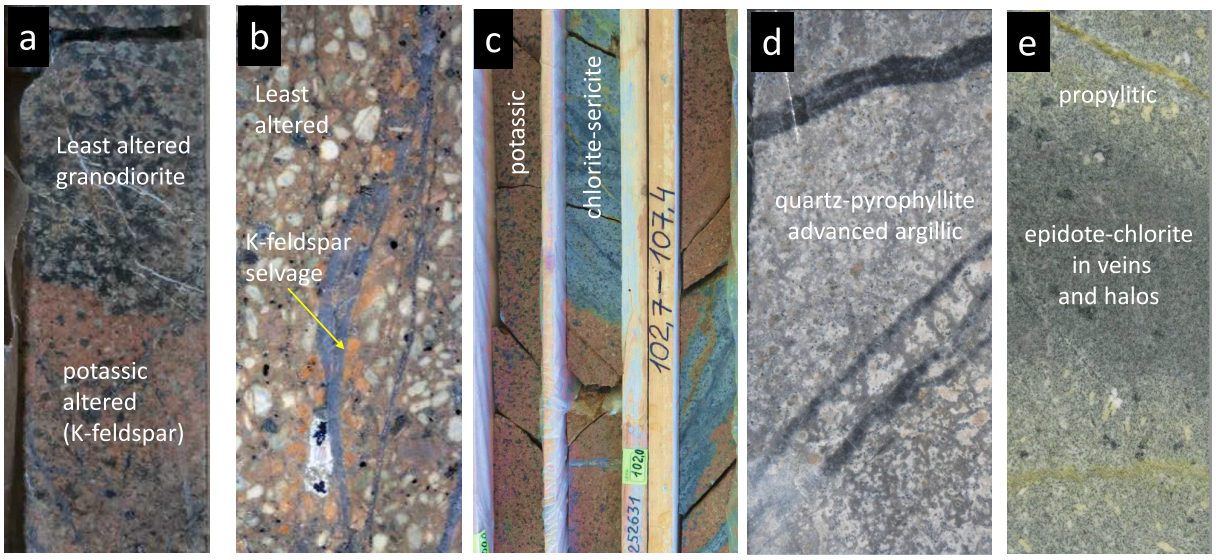

Fig. 3. Examples of alteration types in drill core. a) least altered granodiorite in contact with potassic (pink K-feldspar) pervasive altered granodiorite, the pink colouration is due to hematite dusting in alteration K-feldspar (FOV = 6 cm). Peschanka DHP18-123, 150 m. b) bornite-bearing quartz vein with orange K-feldspar vein-alteration selvage cutting a least altered monzonite porphyry (FOV = 3 cm). Peschanka DHP18-123, 165 m. c) pink K-feldspar rich potassic altered monzonite overprinted by pervasive chlorite-sericite alteration (green–blue) (FOV = 24 cm). Peschanka DHP18-152, 102 m. d) intense pervasive quartz-pyrophyllite alteration with quartz-sulfide veins (photo Huayong Chen, FOV = 8 cm)) e) propylitic alteration of andesite with vein alteration of epidote-bearing veins (apple green) and epidote-chlorite halos (light green) (FOV = 5 cm). El Teniente, Chile (photo Mike Baker).

alteration, and c) pervasive alteration. This means that in many cases a given sample, or 1 or 2 m length of core, may contain hydrothermal alteration assemblages in veins and their halos, or in selective paches, with apparently less- or least-altered porphyry assemblages between the veins and patches. In order to satisfy this situation, it becomes necessary to focus on overprinting alteration assemblages; for example, sericitic alteration overprinting potassic alteration, or propylitic alteration overprinting fresh least altered porphyry compositions. But this approach depends on the scale of sampling, usually one or two meters for drill core in this study. The alteration terminology commonly employed depends if the mineral concerned is part of a single assemblage or is overprinted. In mapping alteration, Sillitoe (pers comm) states that the predominant assemblage dictates the alteration type designation. If two assemblages occur together in roughly equal proportions, then it is mapped as a hybrid alteration, say potassic-sericitic. This would, I think, be common practice (Sillitoe, pers comm). Specific examples of porphyry related alteration and vein overprinting are given in Fig. 3 and are discussed later in more detail.

3. Determining least altered porphyry compositions

The composition of the host porphyry or country rock host rock has a significant control on the alteration type and zonation developed in and around the porphyry system (Hollister, 1974). Consequently, it is first necessary to establish the composition of the least altered host porphyry or porphyries in any given example and determine where those compositions will plot in geochemical space. Seedorff et al (2005) classified the porphyry compositions associated with porphyry Cu deposits as tonalitic-granodioritic, quartz-monzonitic-granitic, monzonitic and syenitic. Here I have reduced the discussion to the three most common groups 1) diorite and quartz diorite, 2) granodiorite, and 3) monzonite and quartz-monzonite. Based on data from Seedorff et al (2005) and Leveille and Stegen (2012) for the SW USA porphyry province and Sillitoe and Perello (2005) for the Central Andes porphyry province diorite and quartz-diorite compositions are present in 13 % of the economic porphyries, granodiorite in 46 % and monzonite and quartz-monzonite in 41 %. The compositional fields for these three groups have been determined using the database compiled by Gard et al., (2019), which contains 38,760 whole-rock analyses of granitoids, which have been classified using the TAS system of Middlemost (1994). Although this database was produced for least altered igneous samples, it is reasonable to assume that a percentage of the original samples selected are altered to some degree. Thus, I have chosen the most-dense distribution on the AI-CCPI diagram as representing the least altered porphyry compositions. This assumption leads to 56 % of the samples being called least altered and 44 % being classified as altered to some degree from their original composition.

The fields for each of the three compositional groups are shown on the AI – CCPI plot (Fig. 4). The assumed least altered, highest concentration of diorite & quartz diorite plot in the top half of the diagram due to more elevated FeO and MgO contents, whereas granodiorite and monzonite plot in the bottom half. The highest density of monzonite samples plots at higher alteration index (40 to 70), compared to granodiorite (25 to 50), principally due to its higher K_2O content. By plotting the alteration mineral compositions or nodes on the edges of the diagram (Fig. 5) it is possible to show several alteration trends, for example from a typical least altered monzonite towards K-feldspar, white-mica, white-mica-chlorite, chlorite-carbonate or epidote-carbonate representing alteration trends related to the specific alteration type (Fig. 5).

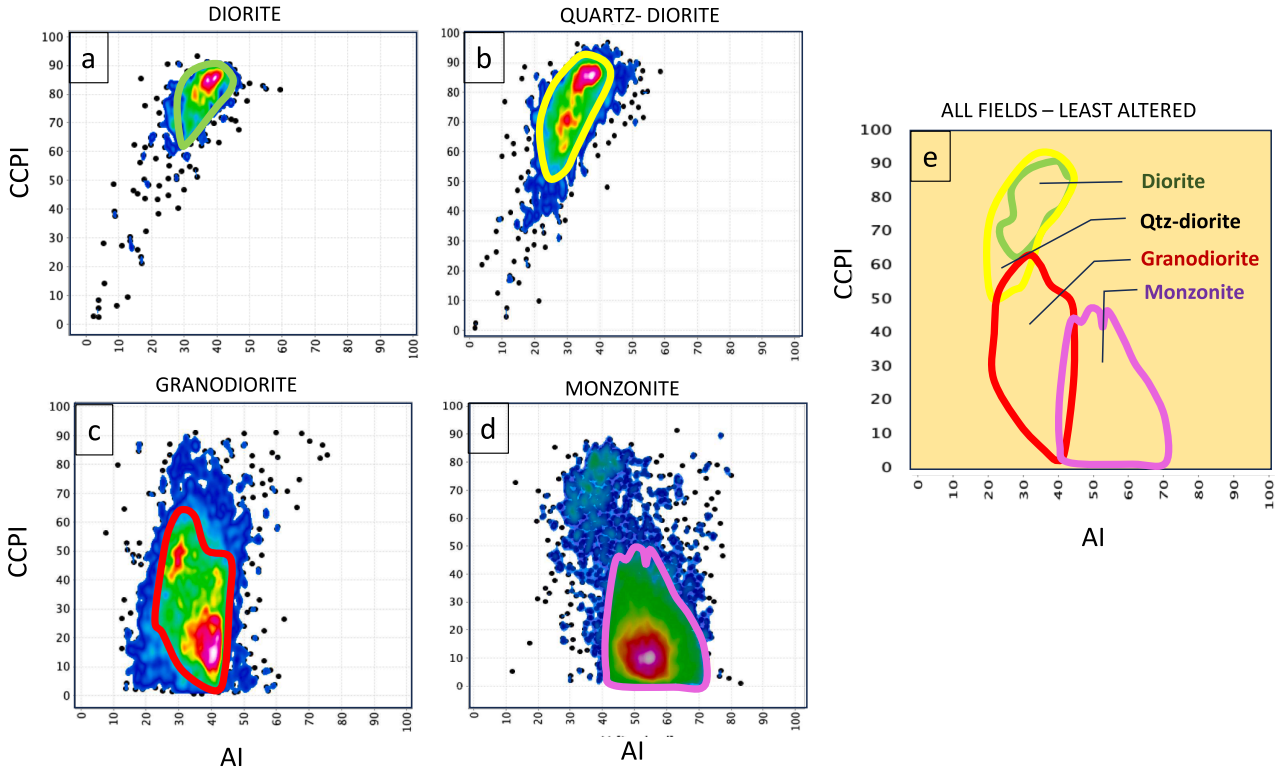

Fig. 4. Fields for the major compositional types of granitoids from the Gard et al (2019) database, plotted in the AI vs CCPI diagram; a) diorite, b) quartz diorite, c) granodiorite, d) monzonite, e) all fields. Colors from blue to red-white indicate increasing density of plotted samples. The monzonite grouping includes monzonites, monzogranites, monzodiorites and biotite granite. The granodiorite grouping includes granodiorite and tonalite. The thick red line outlines the area of highest sample density for each of the four compositional types. Data outside the red outlined fields are either misclassified samples or chemically altered samples of each respective type.

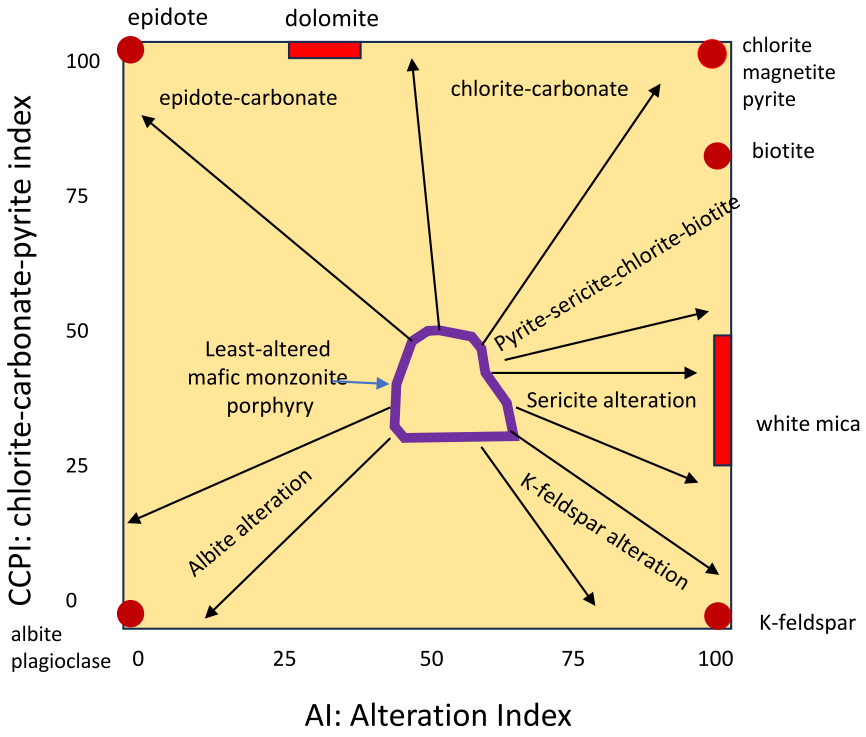

Fig. 5. AI vs CCPI diagram with alteration mineral nodes and trends of some common alteration assemblages based on an initial hypothetical mafic monzonite porphyry parent. White mica is represented as a bar which takes into account the variation in the CCPI axis from muscovite to phengite whereas the dolomite bar represents the variation in the AI axis between dolomite and ankerite.

Throughout the manuscript I have used sericite and sericitic for the alteration type related to the diagrams as they are the terms used mainly by previous authors to describe alteration types. I have used white mica as the mineral node on the diagrams as this covers all forms of the mineral with the general composition of $KAl_3Si_4O_{10}(OH)_2$.

4. Case study 1 – Granodiorite-Monzonite Type: Peschanka porphyry copper Deposit, eastern Russia

The Peschanka porphyry copper–gold-molybdenum deposit is located in western Chukotka, Russia, approximately 250 km southwest of Bilibino (Fig. 6). Initially discovered in 1973, the deposit has been evaluated by drilling in a number of campaigns from 1970′s to present time, and is being developed for production by the Baimskoye company. Chitalin et al (2012) reports an indicated resource of 1.2 billion metric tonnes grading 0.53 % Cu, 140 ppm Mo and 0.29 g/t Au.

4.1. Peschanka geology and mineralisation

The following description of the deposit is summarised from Chitalin

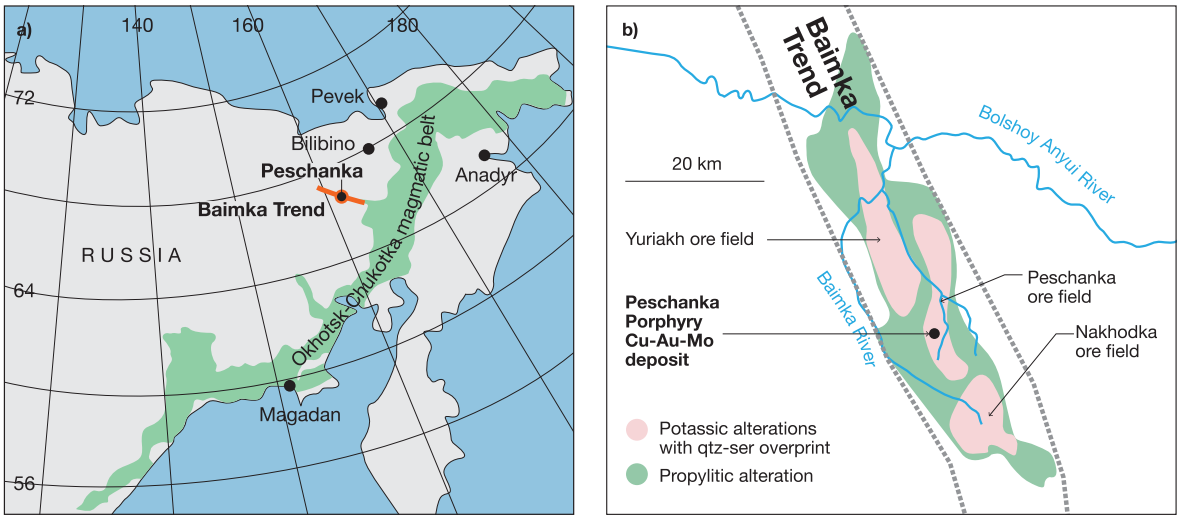

Fig. 6. A) location of the peschanka porphyry copper deposit far eastern russia, b) the baimka trend with location of the peschanka ore field and peschanka deposit. pink is predominantly potassic altered rocks and green is predominantly propylitic altered rocks (fromChitalin et al., 2012).

et al (2012).

The Peschanka deposit lies to the east of the Cretaceous Okhotsk–-Chukotka magmatic belt of the Andean type (Fig. 6) on a major regional north-west structure termed the Baimka trend. The local ore-bearing, altered Early Cretaceous intrusive rocks of the Yegdygkych pluton comprise monzodiorite and monzonite, quartz monzonite, and syenite porphyries (Figs. 6 and 7). The deposit comprises veinlet – stringer–disseminated mineralization that forms a linear stockwork extending for 7000 m north–south and reaching 700–1500 m in width (Fig. 7a). Vertical, inclined, and horizontal zones of high-grade mineralization are traced within the stockwork. Potassic alteration envelopes the stockwork, surrounded by propylitic alteration (quartz-–epidote–actinolite–chlorite– prehnite–albite) which forms an outer aureole about 1 km wide. Later ore-bearing zones of sericitic alteration (quartz– sericite–illite–chlorite) are superimposed upon both propylitic and potassic altered rocks. The sericitic zones vary from 1 mm to over 20 m in thickness and may occupy linear zones of K-feldspar alteration. Chitalin (2012) considers that the linear, steeply dipping zones of high-grade copper mineralization which strike north–south along the centre of the deposit (Fig. 7a), as well as diagonal and low-angle ore zones, were formed as a result of reactivation of previously existed permeable zones. The ore-bearing hydrothermal solutions are assumed to have migrated through these conduits into the quartz–sericite and quartz stockwork, precipitating ore minerals. Sulfides are zoned in the main deposit, consisting of a bornite core surrounded by consecutive bornite–chalcopyrite, chalcopyrite, chalcopyrite–pyrite, and pyrite zones (Fig. 7b). Bornite and chalcopyrite occur in the zones of both potassic and sericitic alteration (Chitalin, 2012).

4.2. *Peschanka drill-hole database*

The drilling assay database provided for this study comprises multielement data on 1,352 drill holes for a total of 64,585 assay intervals. Analyses were Au by fire assay and other elements by 4-acid digest ICP-EOS (ICP40B package) at the SGS Lab in Moscow.

Using the geochemical database, the first task in the study of alteration geochemistry of a porphyry deposit is to determine the composition of the least altered porphyries and in particular the causative porphyry. In most cases the porphyries are extensively altered and immobile elements such as Sc, Th, Ti, Zr, V, Al, Nb and Zr may be used as the means of arriving at the least altered porphyry composition (Fig. 8, Halley, 2020). By itself, this approach is useful to separate porphyries of different composition (Fig. 8 d, e), but provides little information about the degree of alteration. I prefer to use the AI– CCPI diagram (Figs. 4, 5) to determine how the full dataset plots with respect to both the alteration mineral nodes and the least altered composition of major porphyry compositions from the Gard et al (2019) database (Fig. 8a). This figure shows a mass of data covering most of the diagram, but with three areas with the highest data density designated P1, P2 and P3. P1 and P2 overlap the fields of least altered granodiorite and monzonite, whereas P3 overlaps the least altered diorite field deduced previously (Fig. 4). The remainder of the data that plots outside the areas of P1, P2 and P3, represent different assemblages of alteration (Fig. 5). However, this diagram provides little useful evidence to assist in separating the data into potassic, propylitic or sericitic fields. Fig. 8b, shows that in general terms the potassic and sericitic alteration plots on the right side of the diagram, whereas propylitic alteration plots on the left side, however there is too much overlap of the alteration fields for any useful discrimination.

A starting plot preferred by Halley (2020; 2021) is the molar ratios of Na/Al versus K/Al (Fig. 9) originally proposed by Davies and Whitehead in (2006). On this diagram (Fig. 9) the least altered monzonite (LAM) data defined in Fig. 8a (P1 and P2 combined), are concentrated in the area bounded by molar 0.3 to 0.7Na/Al and molar 0.1 to 0.4 K/Al, whereas the least altered diorite (LAD), extends from 0 to 0.25Na/Al and 0 to 0.25 K/Al. As discussed in Halley (2021), the data concentrated around the white mica node at molar 0.3 K/Al (yellow data), represents

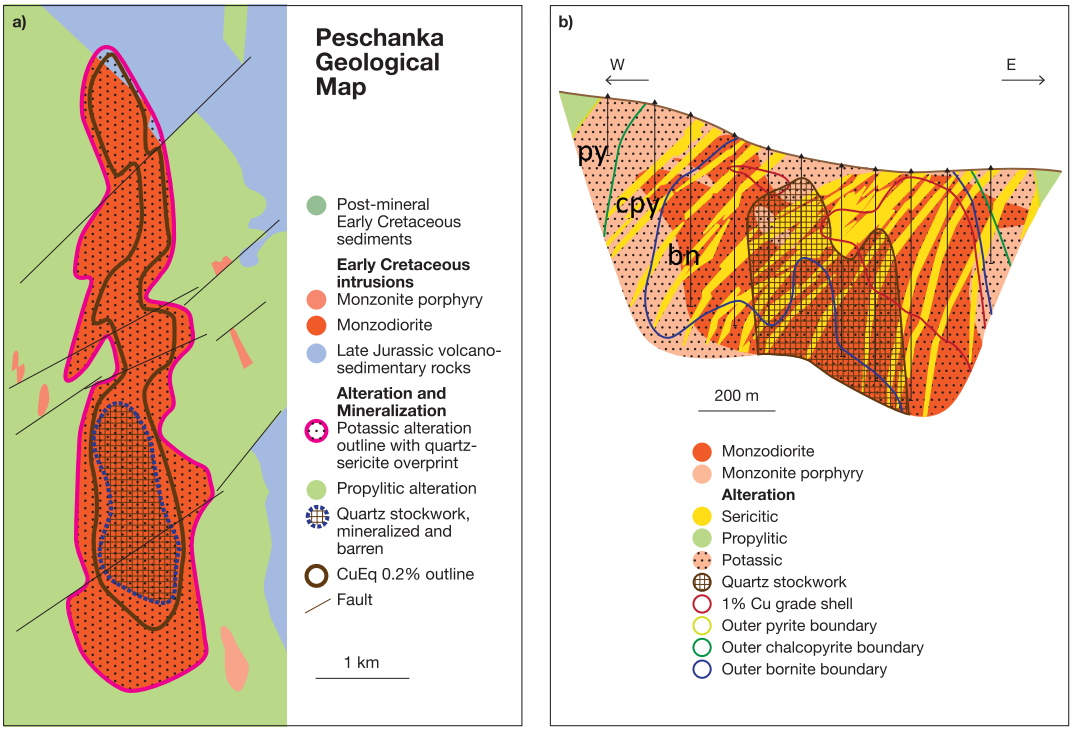

Fig. 7. A) geological sketch map of the peschanka porphyry copper deposit (adapted fromChitalin et al., 2012), b) Geological cross section of the main oredody, Peschanka (adapted from Chitalin et al., 2012). Abreviations; py-pyrite, cpy-chalcopyrite, bo-bornite.

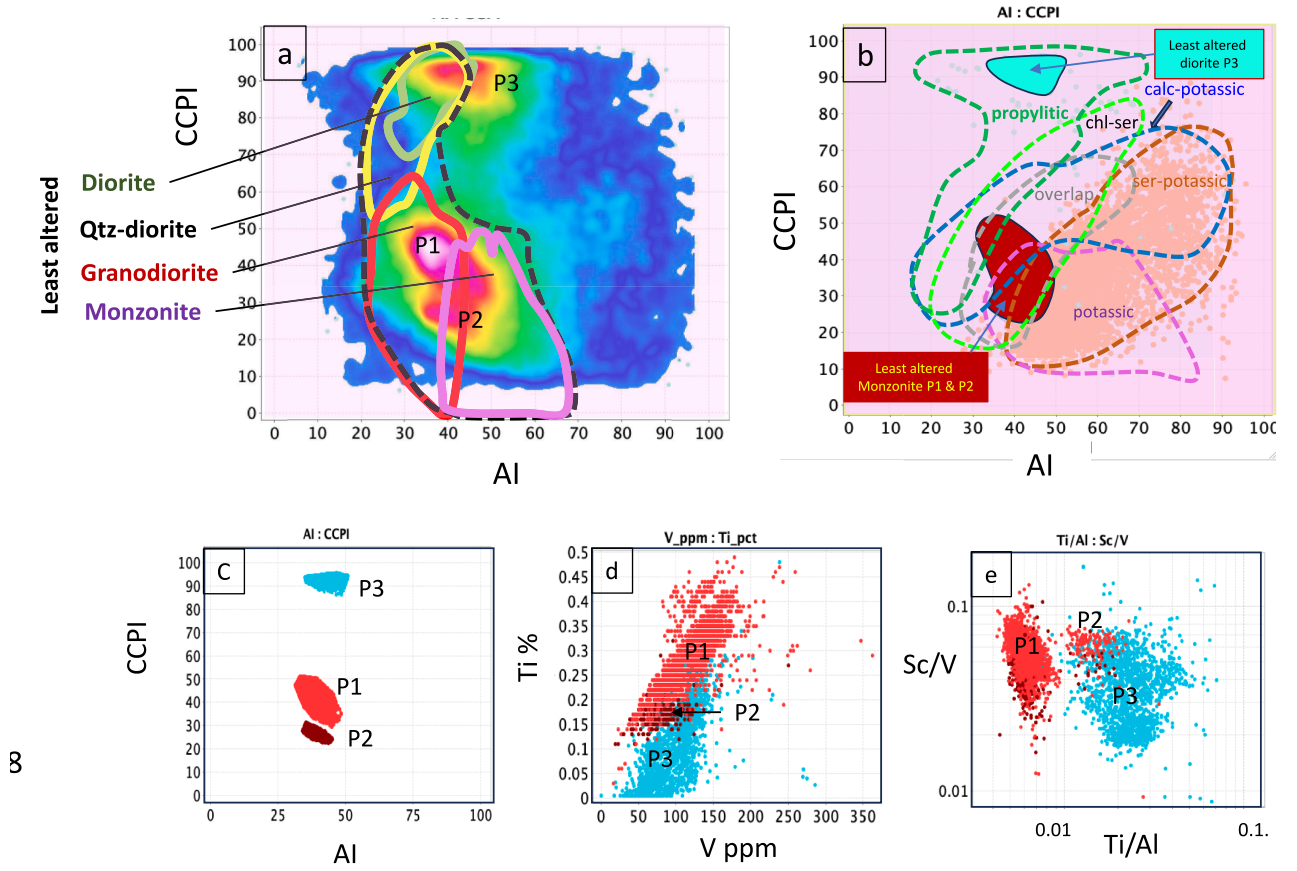

Fig. 8. A) peschanka drill hole geochemical data plotted on the ai-ccpi diagram. colours from blue to red-white are increasing density of sample points. the high density of samples plotting in or overlapping the least altered fields for selected igneous compositions fromGard et al (2019) (Fig. 4) are interpreted to be the least altered porphyry compositions at Peschanka (designated P1, P2 and P3). b) Fields of alteration type at Peschanka plotted on the AI vs CCPI diagram showing extensive overlap and indicating this diagram is of little use in determining alteration type. The alteration fields have been derived from Fig. 10. c, d, e) Immobile element plots (d,e) for the three compositional least altered porphyries compared with the AI-CCPI plot (c) at Peschanka.

the field of high concentration of white-mica, indicating sericitic alteration is dominant in those samples. The trend of data to higher K/Al ratio from white-mica toward biotite and K-felspar (pink data points) represents samples with potassic alteration, and the trend to lower K/Al towards the origin (pyrophyillite, kaolinite, chlorite and dickite, mauve data points) represents samples with advanced argillic alteration. Data points plotting between the white-mica and least altered end-members (orange data points, Fig. 9b) represents samples with weak variable sericitic alteration of the porphyry, trangressing to an assemblage domminated by albite-K-feldspar. Above this field the data represent samples with varying proportions of plagioclase-K-feldspar-biotite and white-mica, whereas below the sericitic field the data plots in the propylitic field (dark green data points) of chlorite-epidote-actinolite-plagioclase. The trend of increasing Na/Al ratio toward the K-feldspar-albite line represents weakly altered samples with an increasing concentration of a mixture of K-feldspar and albite. This plot effectively separates most of the known alteration types in porphyry copper deposits, except for the overlaps between propylitic, chlorite-sericite and advanced argillic assemblages at low molar K/Al ratios of < 0.25. To better achieve this separation, I propose the plot K/(K + Al) versus (K/(K + Ca) (weight percent ratios, Fig. 10). This diagram separates alteration minerals with Ca (e.g., epidote, actinolite, calcite, anhydrite) from those without Ca (e.g. pyrophyllite, kaolinite, chlorite, alunite, albite). It also enables a sodic-calcic field to be separated out from the propylitic field, being defined by K/K + Ca) < 0.4, Na > 2 wt% and Ca from 1.5 to 5 wt%., and defining the field of albitisation of plagioclase.

4.3. *Selection of alteration fields in the PCD diagram*

Because the PCD alteration diagram in Fig. 9 is a summary of alteration assemblages that form over a range of temperatures, from hydrothermal fluids with a range of compositions, altering rocks with a range of compositions then it is not possible to produce a set of alteration fields and boundaries that represent all hydrothermal and host rock conditions for all deposits. The diagram produced (Fig. 9) is thus an approximation to represent alteration fields for the most common set of conditions in porphyry copper genesis.

Three approaches were employed to determine the boundaries between alteration fields. 1) The positions of the alteration mineral nodes are the primary determinant for defining an alteration field. For example, samples with potassic alteration must plot in close proximity to either the biotite node or the K-feldspar node or both biotite and K-feldspar. Samples with advanced argillic alteration must plot in proximity to the mineral nodes for pyrophyllite and kaolinite or between pyrophyllite and alunite. The possible presence of Na-alunite results in the advanced argillic field expanding down the left-hand side of the diagram. Samples classified as sericitic-potassic plot in proximity to the white mica node, and samples classified as propylitic plot in proximity to the epidote node. 2) The initial boundaries selected by this process were checked by plotting the positions of well characterised samples where petrology, SWIR analysis and chemical analysis have been previously published (e.g. Pacey et al 2020, for Northparkes district). There are limited numbers of published samples that satisfy this requirement,

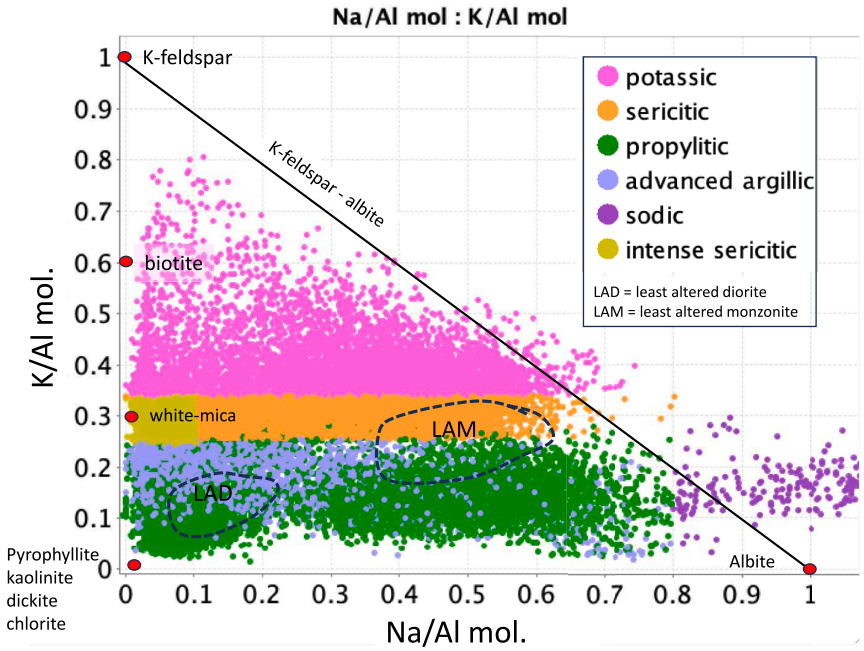

Fig. 9. Peschanka geochemical drill database plotted on the molar Na/Al vs K/Al after the procedure described in the text and from Halley (2021). This enables definition of the major alteration types, but cannot discriminate propylitic from advanced argillic and sericite-chlorite. Outlines of the fields of Peschanka least altered diorite LAD (P3) and least altered monzonite LAM (P1 & P2) are also shown.

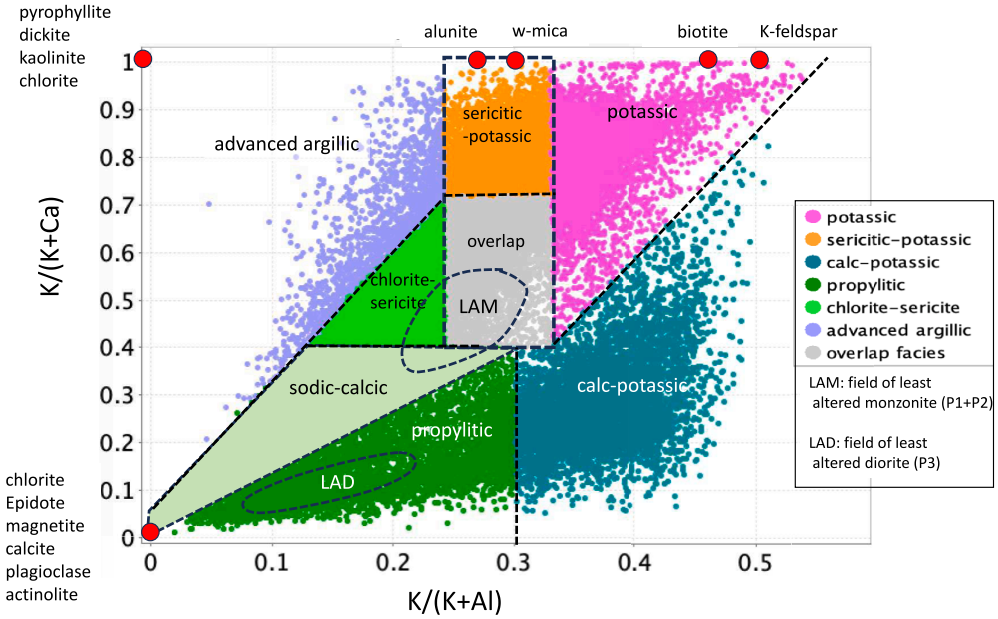

Fig. 10. Peschanka geochemical drill database plotted on the K/(K + Al) vs K/(K + Ca) diagram. The alteration fields are defined by a combination of the classification derived from Fig. 9 and the positions of mineral nodes in this diagram. For example, the advanced argillic type is defined as between the nodes of pyrophyllite, alunite and chlorite. Sericitic-potassic is a transitional type that commonly includes sericitic overprinting potassic with K/(K + Ca) > 0.7. The overlap type includes weak alteration of the monzonite porphyry by overprinting of sericitic, propylitic or potassic assemblages. Chlorite-sericite type is the Ca-poor field of propylitic alteration excluding epidote and actinolite ie with K/(K + Ca) ratio > 0.4. The boundaries on this diagram are not considered permanent and should change as more case study data becomes available.

however this process led to minor changes in boundary positions. 3) Finally, the MINSQ program was used to calculate mineral percentages of selected samples that were plotted based of their chemical analysis (discussed later in section 8). This approach provided good verification for the initial alteration fields selected, and led to further changes in the field boundaries in Figs. 9 and 10. In summary, the final boundaries were selected by an iterative process that employed all three approaches discussed above.

The boundaries between alteration fields produced in this way are not fixed, but will shift slightly due to changes in the composition of the

alteration minerals, particularly white mica and chlorite. At this stage the diagram appears to effectively separate advanced argillic from propylitic alteration, by the introduction of Ca into the ratio on the vertical axis; calcium being generally high in propylitic alteration and leached out during advanced argillic alteration. This diagram also better defines the calc-potassic type, the chlorite-sericite type, the sodic-calcic type and enables an area for skarn alteration, toward the bottom of the plot. White-mica and chlorite predominate above the sodic-calcic field and outline the separate field of the sericite-chlorite alteration (or SCC of Sillitoe, 2010). Due to compositional variations in white mica which effect the minerals K/(K + Al) ratio, it is not possible to define a separate sericite alteration field, and thus the field of sericitic-potassic alteration is defined between K/(K + Al) ratio of 0.24 and 0.33 The lower part of this field is designated an overlap area of a weakly altered assemblages including white-mica, K-feldspar, plagioclase, chlorite, albite, biotite and anhydrite. By plotting the full Gard et al (2019) dataset for least altered granitoids on the same axes (K/(K + Al) versus (K/(K + Ca); Fig. 11), shows diorite and quartz diorites plotting close to the origin, with the data for granodiorites plotting in a continuum at higher K/(K + Al) and K/(K + Ca) and extending to monzonite at the highest K/(K + Ca) values from 0.6 to 1.0 (Fig. 11). The least altered diorite composition overlaps with the sodic-calcic alteration field, whereas least altered monzonite is centred on the potassic field, extending into the potassic-sericitic and overlap alteration fields.

4.4. Peschanka, relating Cu grades to alteration type

An additional strength of this alteration classification diagram is that when the alteration classification is applied to down-hole drill plots the geologist log or SWIR analysis can be compared to the alteration type computed by this method based on the drill core geochemistry. It is unlikely that these two approaches will produce a perfect match as the scale of observation, scale of measurement and minerals detected will commonly vary according to the method employed. The comparison is shown for two drill holes from Peschanka (Fig. 12a). In DHP15 −057 the log determined by SWIR and visual logging from the Peschanka drill hole database, shows a change downhole from propylitic (0 to 100 m), to potassic with intervals of dominantly sericitic (100 to 320 m) to dominantly potassic (320 to 650 m). The geochemical classification based on Fig. 10, gives a similar but more complex change in alteration type. Chlorite-sericite type dominates 0 to 125 m (compared to propylitic), then follows a mixed zone of potassic-sericitic and transitional overlap (compared to potassic over-printed by sericitic), and finally dominantly potassic, with both methods in near agreement. Drill hole DHP15-096 shows a somewhat similar comparison, except the sericitic-potassic is more dominant using the geochemical approach compared with potassic in the company alteration logs. Both holes suggest that the best copper grades are associated with the sericitic-potassic type, which is in agreement with observations by Chitalin (2012) who states that the highest grades of Cu, Au, Mo are related to north–north-east- and south-east trending phyllic (sericitic) zones, which commonly over print the potassic zone (Fig. 7b).

Plotting the complete Peschanka drill dataset of samples with greater than 0.5 % Cu (Fig. 12b), indicates the majority of high-grade copper mineralised samples reside in the sericitic-potassic field extending into the potassic field with high K/(K + Al) ratio exceeding 0.33 and the chlorite-sericite field with K/(K + Al) < 0.24 (Fig. 12b). A second less dense population plots in the calc-potassic field due to more elevate Ca concentration, and may be sourced from the monzodiorite porphyry recognised as LAD in Fig. 9,10 and 12b. The occurrence of good grade copper in the sericitic-potassic field (Table 1), agrees with the drill hole observations (Fig. 12a), but was somewhat unexpected, as it is commonly reported that copper mineralisation is best developed in the potassic alteration (Meyer and Hemley, 1967; Sillitoe, 2010). Without evidence on the timing and paragenesis of white mica it is difficult to be confident about this relationship. However, the original alteration zonation study of Lowell and Guilbert (1970) places the Cu-bearing ore shell at the overlap between the potassic and phyllic (sericitic) zones in the SW USA porphyries. Bouzari and Clark (2006) and Sillitoe and Gappe (1984) also report that some deposits (e.g., Cerro Colorado, northern Chile and many Phillipine porphyry copper deposits) have increased Cu grades where chlorite-sericite alteration overprints potassic alteration zones. It is possible that the elevated copper was initially in the potassic zone before it was overprinted by sericite alteration, however this does not explain the fact that the potassic alteration without significant sericite, commonly has less Cu (but not

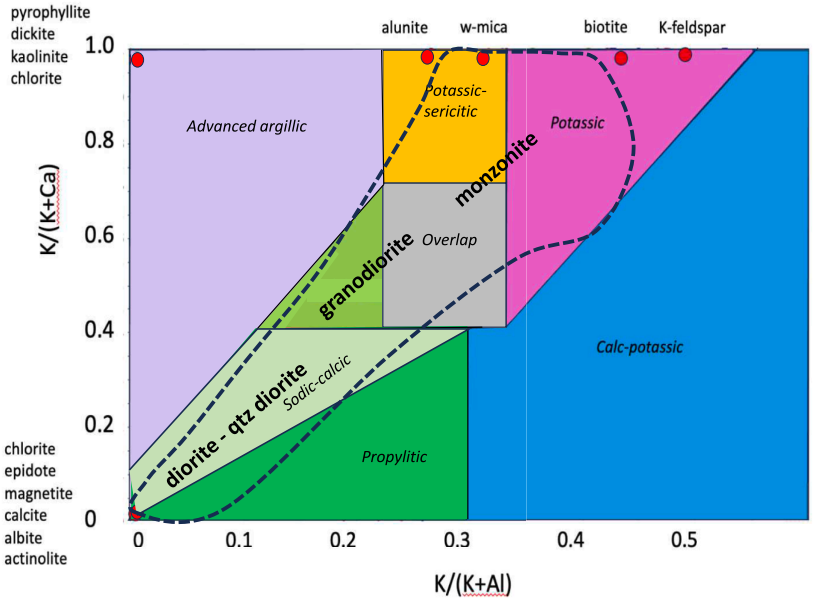

Fig. 11. The field of least altered felsic igneous rocks (black dashed line) from the database of Gard et at (2019) plotted on the K/(K + Al) vs K/(K + Ca) diagram with the alteration type fields from Fig. 10. The fields for least altered diorite – quartz diorite, granodiorite and monzonite are designated.

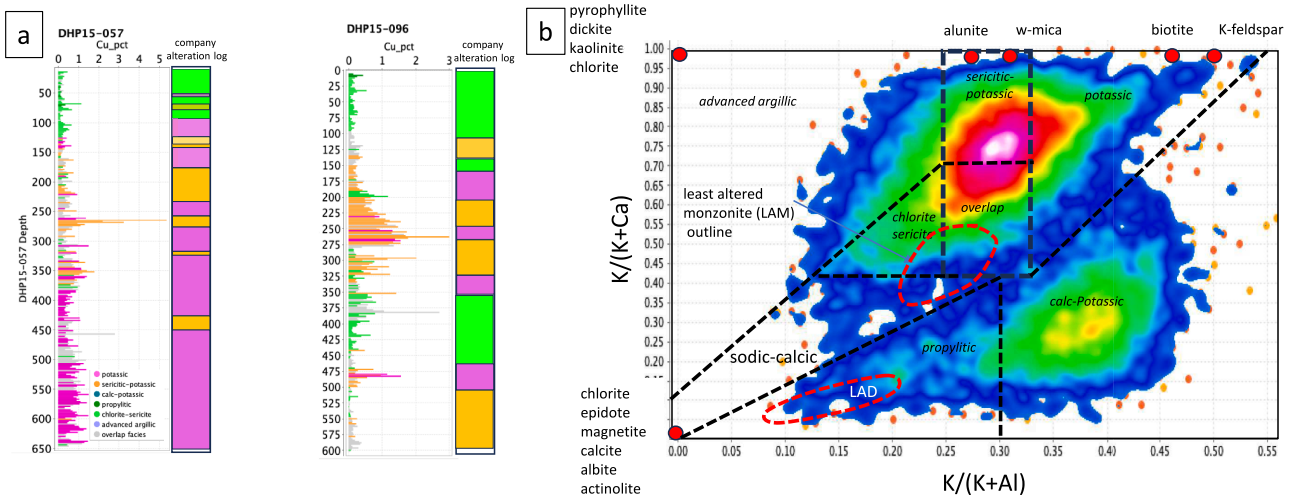

Fig. 12. A) comparison of down-hole cu grade and change in alteration type derived fromFig. 10 (coloured bar chart) compared with a summary of alteration logged in the Peschanka database. The colours for alteration are same as for Fig. 10. Both figures show Cu grades > 0.5 % are dominantly in the potassic overprinted by sericitic type (designated potassic-sericitic). b) Peschanka samples with Cu > 0.5 % plotted on the K/(K + Al) vs K/(K + Ca) diagram. The colours from blue through red to white represent increasing density of samples, the most dense being in the sericitic-potassic field. Least altered fields for Peschanka monzonite (LAM) and diorite (LAD) are outline by the dashed white and black lines. Fields for alteration type are from Fig. 10.

Table 1
Peschanka mean Cu and Au concentration for each alteration type determined from Fig. 10.

Alteration facies	Cu %	Au g/t	Nos. samples	Percentage of samples
Potassic	0.54	0.44	5642	13.2
Sericitic-potassic	0.64	0.35	7357	17.2
Calc-potassic	0.52	0.32	6207	14.6
propylitic	0.14	0.05	9805	23.0
Chlorite-sericite	0.21	0.09	4675	11.0
Advanced argillic	0.51	0.22	1553	3.6
Overlap	0.38	0.22	7413	17.4

Au) than the sericitic-potassic type (Table 1).

The triangular diagram Cu-Fe-S is an alternative way to present the relationship of Cu distribution in each of the major alteration type (Fig. 13 a to f). The linear trend between biotite (+/- magnetite) and bornite is seen as the major control on copper grades in all four major alteration types of potassic, calc-potassic, potassic-sericitic and chlorite-sericite type (Fig. 13a to d). Chalcopyrite plays a lesser, but important control.

5. Preliminary modelling of alteration trends

Simple modelling of the alteration trends relating to overprinting alteration of a least altered monzonite was undertaken to confirm our estimates of alteration fields on the graphical plots discussed previously. A typical least altered monzonite composition was selected from the Gard et al (2019) database, and compositions for strong potassic, sericitic, propylitic and advanced argillic were selected from the case studies (Table 2). The altered porphyry compositions were selected to have medium to intense alteration mineralogy from the Peschanka and Onto drill hole databases. The trajectory of the alteration path in each case in Fig. 14 was determined by mixing the least altered monzonite porphyry with increments of 10 % wt for wt of the altered porphyry from Table 2, up till 90 % altered porphyry and 10 % unaltered porphyry were reached.

Trends were modeled for:

- Potassic alteration overprinting least altered monzonite (two models)
- Sericitic alteration overprinting least altered monzonite
- Propylitic (+ sodic-calcic) alteration overprinting least altered monzonite
- Advance argillic alteration overprinting sericitic alteration (two models)
- Calc-potassic alteration overprinting least altered monzonite.
- Sodic alteration overprinting least altered monzonite

The modeled alteration trends from 10 % overprinting to 100 % overprinting are shown in Fig. 14. These model trends support the fields chosen for the respective alteration type in Fig. 10. They also demonstrate that for potassic, sericitic and calc-potassic alteration of a monzonite, there needs to be at least about 10 % to 20 % alteration overprinting of the monzonite porphyry before significant alteration is recorded on the respective plots. This means that the method does not readily recognize weak veinlet or selective alteration of less than 10 % to 20 % compositional (mineralogic) change in the porphyry or wall rocks.

6. Case study 2 – Diorite type: Kharmagtai porphyry copper Deposit, Mongolia

The Kharmagtai deposit is a multi-centred porphyry Cu-Au system located 200 km north of Oyu Tolgoi in Mongolia. Xanadu Mines ltd in 2024 reported a total indicated resource of 1,300 Mt at 0.22 % Cu and 0.17 g/t Au (https://www.investi.com.au/api/announcements/xam/a0608eb0-644.pdf). Mine construction is timetabled to start in 2025 with the first concentrate produced in 2027. Porphyry related outcrops, including tourmaline breccias were first mapped in the mid 1970's and a shallow drill-defined resource was established by 1980 (Sharkhuu, 1980, in Kirwin et al., 2005).

6.1. Geology and Mineralisation, Kharmagtai

The following geological summary is from Kirwin et al (2005). The Kharmagtai porphyry copper–gold district is located in a belt of Mid-Palaeozoic arc-related calc-alkaline to high K calc-alkaline igneous rocks known as the southern Mongolia magmatic belt. Geological

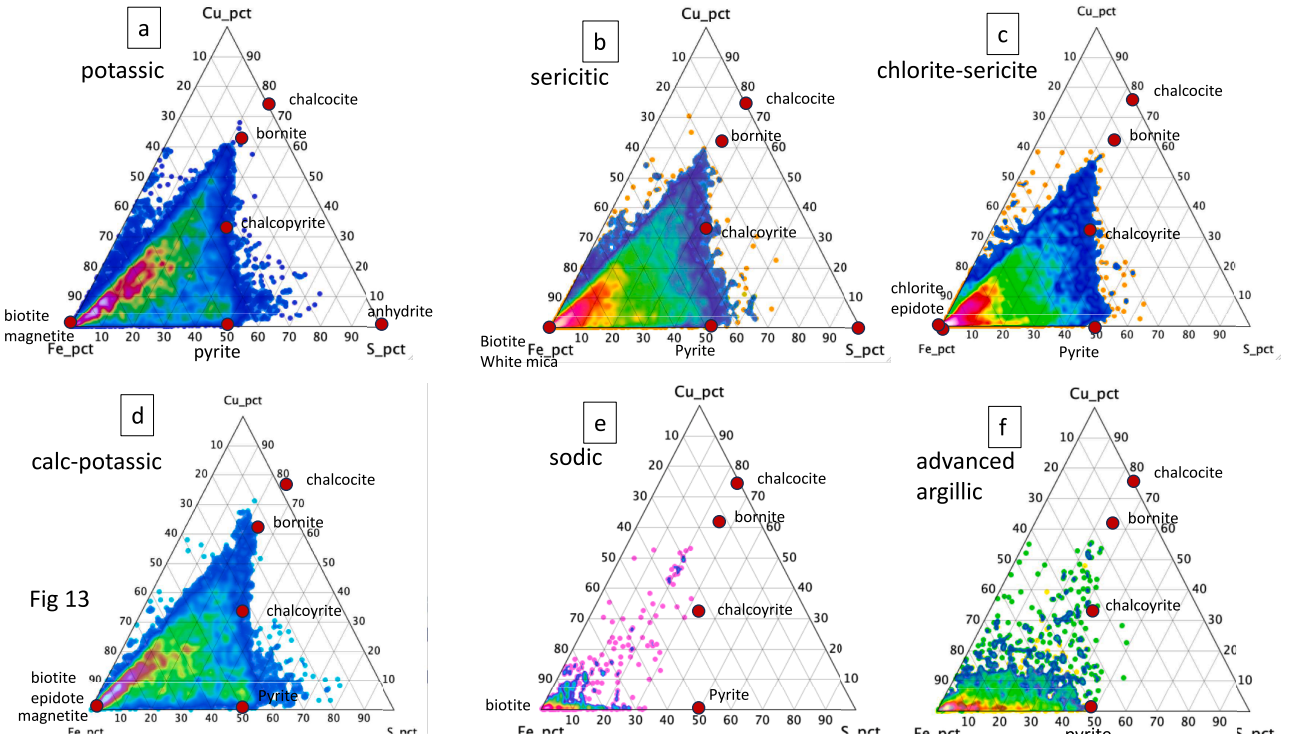

Fig. 13. Peschanka drill hole samples with Cu > 0.5 % plotted on a Cu-Fe-S triangular diagram for each of the major alteration types a) potassic, b) sericitic, c) chlorite-sericite, d) calc-potassic, e) sodic, and f) advanced argillic. The alteration types are defined by their position in Fig. 10.

Table 2
Major element composition of altered porphyries used in the alteration modeling (Fig. 14).

	K2O	Na2O	Al2O3	CaO	FeO	MgO	SiO2
Least altered monzonite	3.95	3.67	13.95	3.37	3.94	2.40	68.72
potassic altered (biotite)	5.65	0.46	14.80	0.52	2.21	1.59	74.77
potassic altered (K-feldspar)	5.78	0.66	8.17	0.34	0.45	0.23	84.37
sericitic altered	1.96	0.08	7.52	0.15	2.16	0.88	87.25
propylitic altered	1.78	2.01	15.77	7.90	6.80	2.87	62.87
advanced argillic altered	0.67	0.24	19.00	2.03	8.74	2.34	66.98
sodic altered	2.35	9.32	13.03	3.60	4.30	1.48	65.92

mapping at Kharmagtai has revealed that much of the area is comprised of Devonian silty clastic sedimentary rocks which have been intruded by a number of monzodiorite and diorite porphyry stocks. Numerous tourmaline breccia pipes are scattered throughout the district, the largest of which has a diameter of 500 m.

Mineralisation and alteration at Kharmagtai is characterised by multiple gold-copper porphyry centres, gold-base metal-bearing breccia pipes and complex structurally controlled silicified zones. Six separate porphyry centres have been defined by drilling, comprising White Hill, Copper Hill, Stockwork Hill, Zaraa, Golden eagle and Zephyr (Fig. 15b, after Potma et al., 2018). The main deposit at Stockwork Hill consists of two gold-bearing quartz-chalcopyrite-pyrite stockwork zones, 100 m apart, hosted in diorite and quartz diorite (Fig. 16). Quartz-sulphide +/- gold veins are considered to represent the main fracturing and veining event. They are filled by assemblages of quartz, chalcopyrite, pyrite, epidote, magnetite, calcite, bornite, chlorite, tourmaline, native gold and possibly biotite. Wall-rock alteration associated with these veins, has a mineralogy of albite + quartz + biotite? + epidote + chalcopyrite + pyrite + trace apatite ‡ magnetite) and has been interpreted as potassic type (Kirwin et al (2005). Tourmaline breccias and diorite breccia are common in the deeper parts of the deposit, where they are variably Cu-Au-mineralised (Fig. 16).

With regard to alteration, Potma et al (2018) maintains that the classic alteration zonation of Lowell and Gilbert (1970, Fig. 1a) is not recognisable at Kharmagtai. They point out that albite alteration is abundant and coincident with significant Cu-Au-rich quartz B-vein stockworks. They observe the stockwork zones at Stockwork Hill to be composed of abundant laminated quartz-magnetite veins with chalcopyrite (B-veins) associate with epidote-magnetite alteration. The laminated stockwork veins have been later re-opened and overprinted by strong chalcopyrite C-veins. Syn to post mineralisation tourmaline breccias are zoned from chlorite-rich cement infill to pyrite then chalcopyrite within the core of the breccia domain (Potma et al., 2018).

6.2. *Kharmagtai drill hole database*

The drill-hole assay database provided by Xanadu Mines included drilling from the six porphyry centres, totalling 1,221 drill holes and 140,763 assay intervals. No spatial coordinate data was available so although alteration cross sections could not be plotted, computed alteration down individual drill holes could be assessed. Only samples from the porphyries were plotted, and the shale country rocks excluded as these have a variable, generally high potassium content that may be confused with potassic alteration. The analytic method was a four acid 48-element package (ME-IC61, ALS) with Au determined by fire assay. About 85 % of assay intervals in the database had full major element analyses and could be plotted on the diagnostic diagrams of AI vs CCPI and K/(K + Al) vs K/(K + Ca) (Fig. 17). These plots demonstrate the major least altered porphyry composition is diorite to monzodiorite (Fig. 17a), with a spread of potassic-sericitic, chlorite-sericite, sodic-calcic and propylitic type, with minor potassic, advanced argillic and

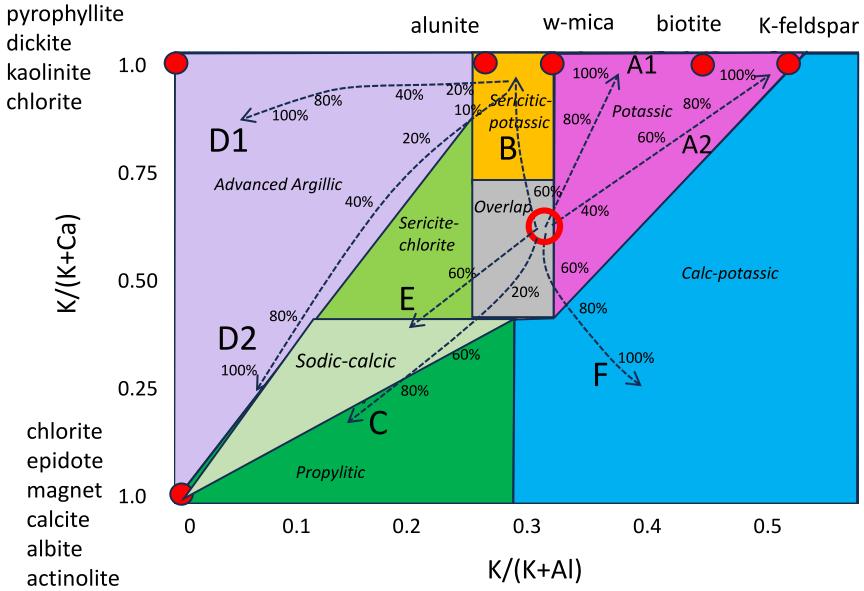

Fig. 14. Trends on the K/(K + Al) vs K/(K + Ca) diagram produced by modelling overprinting alteration: model A1) potassic (biotite dominant) alteration overprinting least altered monzonite; A2) potassic (K-felspar dominant) alteration overprinting least altered monzonite; B) sericitic alteration overprinting least altered monzonite; C) propylitic alteration overprinting least altered monzonite; D1) advanced argillic (with pyrophyllite +/- alunite) alteration overprinting sericitic alteration, D2) advanced argillic (with chlorite and little alunite) alteration overprinting sericitic alteration, E) sodic alteration overprinting least altered monzonite, and F) calc-potassic alteration overprinting least altered monzonite. Red circle represents composition of least altered monzonite. This modelling exercise helps to demonstrate the robust nature of the alteration fields and their boundaries.

calc-potassic type (Fig. 17b). The advanced argillic alteration is confined to porphyries within 40 m of the surface and is most likely due to supergene kaolinite. In the plot of samples with Cu > 0.5 % and Au > 0.5 ppm over the alteration type (Fig. 18a), the highest density of Cu and Au rich samples lie in the sodic-calcic field (72 %, summarised in Table 3) extending into the sericite-chlorite field (14 %), in marked contrast to the previous case study where the highest density of Cu-rich samples are in the sericitic-potassic and potassic fields. The Cu density plot at Kharmagtai, shows an elongate field of high-density Cu > 0.5 % stretching from the origin, across the sodic-calcic field and through the chlorite-sericite field toward the potassic field (Fig. 18a). Although there are reports (Kirwin et al., 2005) of biotite and K-feldspar associated with some of the mineralised quartz veins, in the deposits at Kharmagtai, quartz-sulfide +/- gold veins are reported to be filled with assemblages including quartz, chalcopyrite, pyrite, albite, epidote, magnetite, chlorite, tourmaline, native gold and possibly biotite (Kirwin et al., 2005). This assemblage is not typical of potassic alteration, but due to the presence of albite- epidote-chlorite is more in-keeping with a sodic-calcic alteration assemblage. An alternative interpretation is that because of their calcic nature, diorite porphyries commonly contain epidote (and actinolite) as part of the potassic assemblages.

In summary, this study of the assay database is in general agreement with the statement by Potma et al (2018) that the alteration at Kharmagtai does not conform to the classic porphyry copper alteration model, of a Cu-rich potassic core. Late stage mineralised tourmaline breccias, which are common in the Cu zone at Kharmagtai also plot principally in the sodic-calcic field, with highest copper–gold grades plotting toward the epidote-albite end of the field, but extending up into the chlorite-sericite field. Compared to the propylitic type alteration, the sodic-calcic alteration, which hosts most of the Cu-Au mineralisation has higher concentrations of albite, but lower epidote and plagioclase. Albitisation of plagioclase appears to be the major process in forming the sodic-calcic alteration. This is expressed in the bulk Na concentration, where Cu-Au bearing sodic-calcic alteration at Kharmagtai has Na > 2 %, whereas the low grade propylitic type has Na < 1 %. Down-hole plots of computed alteration and Cu-Au concentration also demonstrate the relationship of Cu-Au to the sodic-calcic alteration (Fig. 18b).

Drill hole (KHDDH359) through the centre of the mineralisation and tourmaline breccias at Stockwork Hill (Figs. 15 and 18b), shows mineralisation with Cu > 0.4 % and Au > 0.4 g/t coinciding with the sodic-calcic alteration type (0 to 220 m) hosted by the mineralising diorite. The tourmaline breccia intersection from 300 to 470 m commonly has Cu < 0.1 % and Au < 0.1 g/t associated with intermittent potassic, calc-potassic and overlap alteration type. The hole then passes out (470 to 600 m) into higher Cu-Au grades in chlorite-sericite and sodic-calcic alteration.

There are a number of possible reasons for the unusual situation of the bulk of the Cu reporting in the sodic-calcic alteration and chlorite-sericite field rather than the potassic and potassic-sericitic fields which is typical of most calc-alkaline based porphyries.

- The host porphyries at Kharmagtai are diorite and monzodiorite with high CaO of 4 to 6 % and low to medium primary K_2O; 1.5 to 2.5 %, compared to most granodiorite, monzonite and quartz-monzonite with lower CaO from 3 to 5 % and higher K_2O from 3 to 4.5 %, as is the case for the Peschanka monzonite
- Diorite melts may not in all cases produce K-rich ore fluids, due to their low K-content. Diorites are more likely to produce Ca-Na-rich fluids.
- Although the mineralized stockworks and tourmaline breccia contain some potassic phases (biotite and K-feldspar), they are subordinate to sodic and calcic minerals (albite, epidote and plagioclase) and insufficient to move the overall composition of the ore into the potassic field. Ie., the weak potassic overprint is less than 50 wt%, and closer to 10 to 20 % of the rock based on the major element chemistry in the drill database. Estimates of the mean mineralogy of the mineralized (Cu > 1 %) altered diorite porphyry based on the MINSQ method, discussed later, are albite 15 %, plagioclase 12 %, chlorite 14.5 %, epidote 7.5 %, white-mica 7.5 %, K-feldspar 6.5 % and biotite 4 %. World-wide unaltered diorite compositions generally have primary K-feldspar up to 10 % and in monzodiorites up to 35 % (Middlemost, 1986), and thus K-feldspar concentrations of

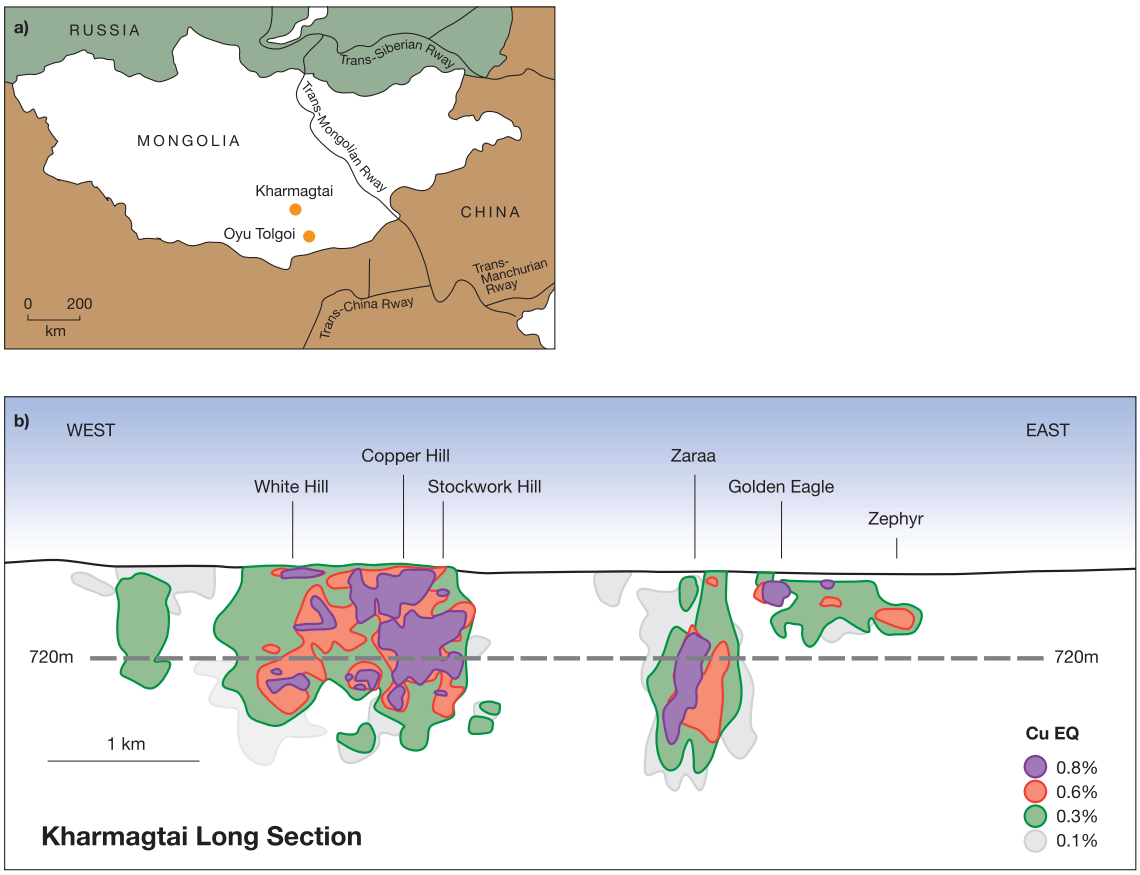

Fig. 15. A) location of kharmagtai and oyu tolgoi in mongolia b) long section of the porphyry cu-au centres at kharmagtai with cu grade contours(https://www.investi.com.au/api/announcements/xam/9da4a5ed-0cb.pdf).

around 5 to 10 %, as in the Kharmagtai mineralized diorites, may not be due to potassic alteration, but rather primary K-feldspar relics in a sodic-calcic albitised monzodiorite porphyry.

- Also, a late chlorite-epidote overprint, if extensively developed in some of the Kharmagtai deposits, would draw the Cu-rich assemblages back to the propylitic field (Fig. 18a).

6.3. *Discussion of the diorite case study*

Hollister (1974) recognised differences between porphyry copper deposits related to diorite porphyry compositions and those related to granodiorite-monzonite compositions. He refered to the two types as the diorite model and the Lowell and Guilbert model (Hollister, 1978), here called the granodiorite-monzonite model. According to Hollister the diorite model porphyries have a core zone dominated by either chlorite or chlorite-biotite, and commonly lack K-feldspar, but contain plagioclase (or albite); these features being similar to those core assemblages in Kharmagtai. The sericitic zone is commonly absent in the diorite type porphyry deposits and copper mineralisation is present in the sodic-calcic and sericite-chlorite alteration zones, compared with granodiorite-monzonite type where the copper mineralisation is in the potassic and sericitic zones (Hollister, 1978). Even though the diorite type porphyry copper core zone is enriched in albite, plagioclase, epidote and chlorite with K-feldspar and biotite at lower concentrations or absent, Hollister (1978) prefered to retain the name potassic zone. I find this very confusing and not approprite for a classification based on mineralogy and lithochemistry. I prefer sodic-calcic alteration as a more approprite term for the mineralised core of diorite-based porphyry copper deposits. To emphasise the role of Ca in the alteration I have plotted the alteration type for Peschanka (granodiorite-monzonite porphyry) and Kharmagtai (diorite porphyry) on a Ca-K-Fe triangular diagram (Fig. 19). This demonstrates that the highest density of samples with Cu $>$ 0.5 % at Peschanka, plot adjacent to the K-Fe side of the triange in the potassic-sericitic alteration field, whereas at Kharmagtai the Cu $>$ 0.5 % samples plot adjacent to the Ca-Fe side of the triangle in the sodic-calcic and sericite-chlorite type.

In his discussion of gold-rich porphyries related to calcic porphyries such as diorites and quartz diorites, Sillitoe (1993) points out that the potassic zone commonly contains actinolite and epidote, in addition to their presence in the propylitic alteration zone. Notwithstanding this observation he maintains that the bulk of the copper and gold is associated with potassic alteration in diorite porphyry systems. In the Maricunga Belt, Northern Chile, Au-Cu porpyry deposits are hosted by diorite and quartz diorite intrusions, where the primarry ore-related alteration assemblage is quartz-chlorite-clay-sericite (here termed chlorite-sericite type) with rare potassic alteration (Vila and Sillitoe, 1991, table 1). This highlights a difference in terminology. Sillitoe and Gappe (1984), Vila and Sillitoe (1991) and Sillitoe (1993), use the potassic or potassic-calcic alteration term based on the presence of biotite and/or K-feldspar and/or actinolite, even when albite, chlorite or epidote are dominant alteration minerals, whereas here the term potassic or potassic-calcic type is based on the fact that potassium is enriched in the rock above the least altered diorite composition, when K/(K + Al) $>$ 0.33 (Figs. 10, 17b).

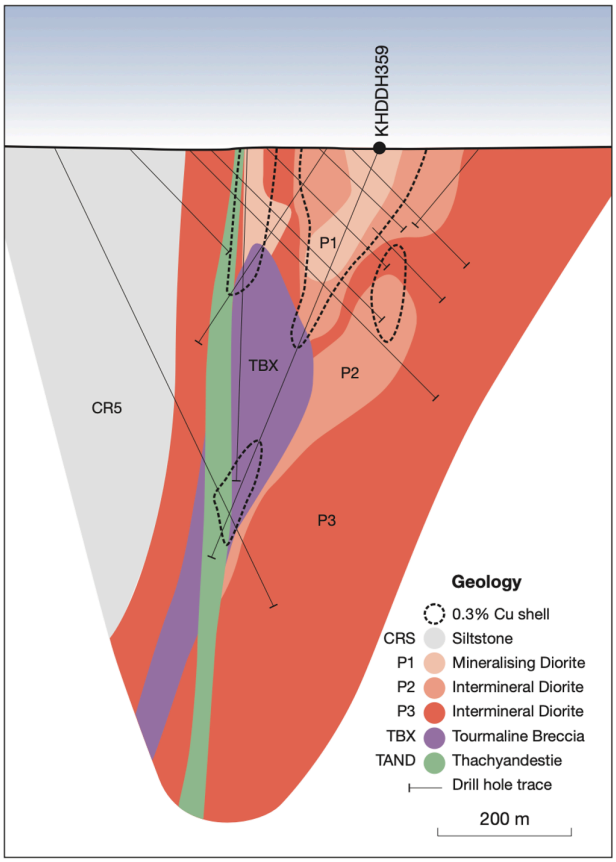

Fig. 16. Typical geological cross section of the Stockwork Hill porphyry copper–gold deposit, Kharmagtai, with selected drill holes (Potma et al., 2018).

7. Case study 3 – Advanced argillic Overprint: Onto porphyry Cu-Au Deposit, Indonesia

Onto is a recent greenfields exploration discovery on the island of Sumbawa (Fig. 20a) which consists of deep porphyry stocks intruding a diatreme breccia and volcaniclastic succession, all overprinted by a high sulfidation advanced argillic alteration type (Burrows et al, 2020, Fig. 20b,c). Following several efforts of systematic exploration starting in 1995, the discovery hole at Onto was drilled in 2013, intersecting 287 m at 0.97 % Cu and 1.13 g/t Au in vuggy-textured residual quartz and quartz-alunite alteration. The deposit has an indicated resource of 0.76 billion tonnes at 0.93 % Cu and 0.56 g/t Au (Burrows et al, 2020).

7.1. Geology and mineralisation at onto

The following geological description is summarised from Burrows et al, (2020).

At the Onto deposit, copper and gold are associated with a series of porphyry stocks that intrude a polymictic diatreme breccia, topped by laminated siltstones, volcaniclastic, pyroclastic rocks, and overlaid by andesite flows (Fig. 20b). The porphyry intrusions formed at shallow depths (≤1.3 km), with quartz veinlet stockworks developed between 600 and 1,000 m below the present surface.

The diatreme breccia, porphyry intrusions, and surrounding andesite sequence have all undergone intense advanced argillic alteration. This alteration is zoned downward from illite-smectite, quartz-dickite to quartz-alunite and quartz-pyrophyllite ± diaspore alteration, determined principally by SWIR (Fig. 20c). Two significant residual quartz zones, one porous and the other silicified, are present at shallow depths, with mineralization starting below the lower silicic horizon.

More than 90 % of the resource lies in quartz-alunite and quartz-pyrophyllite-alunite alteration zones. The mineralization consists mainly of high-sulfidation covellite-pyrite assemblages in open spaces and veins, with covellite being the dominant copper mineral. Although most copper mineralization formed during advanced argillic alteration, about 60 % of the resource at a 0.3 % Cu cutoff occurs in the porphyry stocks, indicating their key role in controlling mineralization. Copper and gold have also been remobilized into surrounding rocks and late intrusions, resulting in consistent grades. Early chalcopyrite-bornite mineralization with potassic alteration is preserved only at the system's margins and contributes around 8 % of the resource (Burrow et al., 2020).

7.2. Onto drill hole assay database

The drill hole database provided by Vale contains 65,366, 2 m assay intervals, from 227 drill holes comprising multi-element analyses,

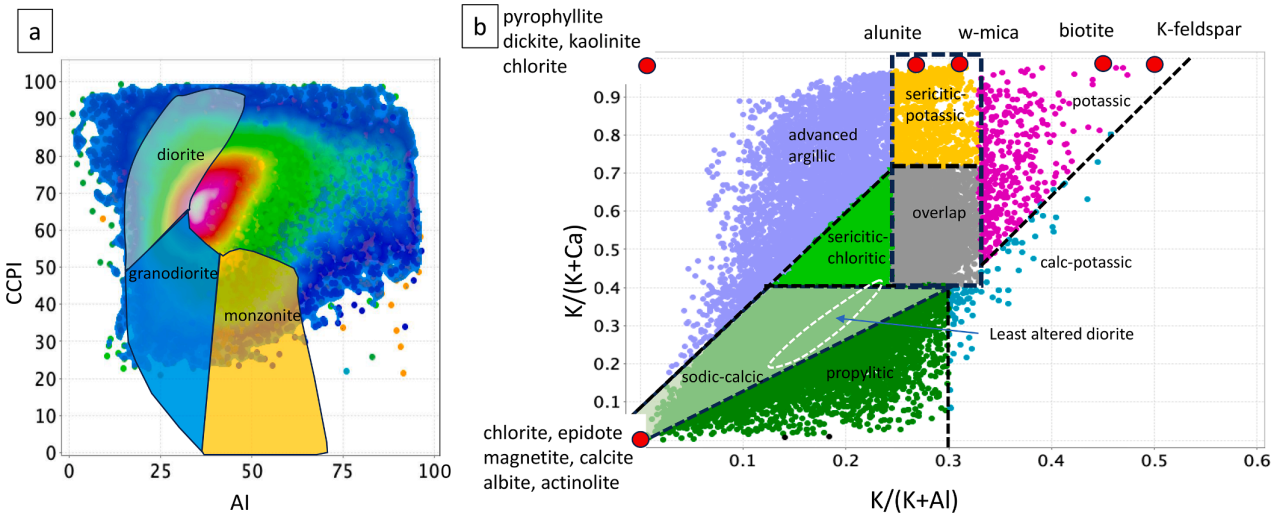

Fig. 17. A) kharmagtai drill hole geochemistry plotted on an ai vs ccpi sample density diagram. the highest density of samples overlap the least altered diorite field. the shift to the right of the high density zone may be caused by a slight enrichment of potassium, leading to a monzodiorite classification. b) kharmagtai drill geochemistry plotted on the alteration type k/(k + Al) vs K/(K + Ca) diagram. The alteration type boundaries are from Fig. 10. The least altered Kharmagtai monzodiorite field is marked by the solid black line.

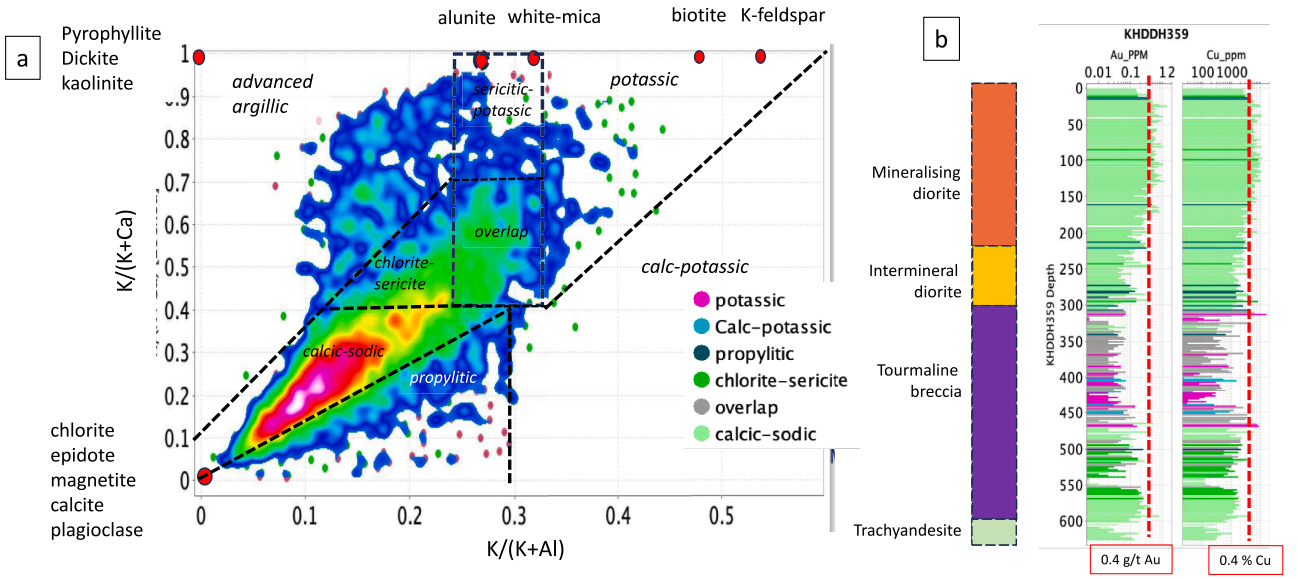

Fig. 18. A) kharmagtai sample density plot on the k/(k + Al) vs K/(K + Ca) diagram for all samples with Cu > 0.5 %. The highest density of samples with Cu > 0.5 % lies in the propylitic field. The alteration type boundaries are from Fig. 11a. b) Stockwork Hill drill hole KHDDH359 through the centre of the deposit (Fig. 16) intersecting mineralised porphyry and tourmaline breccia. Geology log from Fig. 16 and coloured alteration log from Fig. 17b. The mineralised diorite porphyry shows sodic-calcic alteration whereas the tourmaline breccia zone has a mixture of alteration types including potassic, calc-potassic, overlap and sericite-chlorite.

Table 3
Kharmagtai mean Cu and Au concentration for each alteration type using a cutoff of 0.2 % Cu and 0.2 ppm Au (determined from Fig. 17b.).

Alteration facies	Cu %	Au g/t	Nos. samples	Percentage of samples
Potassic	0.82	0.66	62	0.5
Sericitic-potassic	1.66	0.47	123	1.0
sodic-calcic	1.3	0.52	8676	71.7
Propylitic	1.6	0.56	610	5.0
Chlorite-sericite	1.2	0.44	1721	14.2
Advanced argillic	1.7	1.1	377	3.1
Overlap	1.16	0.52	533	4.4

including 36 elements. Analyses were by 4-acid ICP-OES at the Intertek laboratory in Jakarta. All drilled rock types and alteration are represented. The data has been plotted on the AI vs CCPI and K/(K + Al) vs K/(K + Ca) diagrams to compare with the other two case studies (Fig. 21).

The overprint advanced argillic alteration is so intense that no primary porphyry composition is evident in the AI-CCPI plot (Fig. 19a), except for post mineralisation andesitic lavas that cap the deposit. The majority of the drill data plots at high AI and CCPI indicative of advanced argillic alteration. The K/(K + Al) vs K/(K + Ca) plot show a small population of data in the potassic field and much larger population in the advance argillic field (Fig. 21b), however these diagrams do not fully show the significance of the alunite-bearing advance argillic overprint reported by Burrows et al (2020). The presence of alunite is best revealed on a triangular plot of Ca-Fe-S (Fig. 22a, Halley, 2020) where excess S above 50 % S is due to the presence of alunite, and minor covellite and native sulfur in addition to pyrite. Anhydrite is also indicated to be present on this plot, by high sulfur and calcium without high Fe content, but rarely occurs in the same assemblage as alunite (Fig. 22b). Plotting the alunite-bearing assemblage shows the full extent of the advanced argillic alteration, overprinting most of the potassic, sericitic and part of the propylitic alteration as defined by the plot (compare Fig. 21b to Fig. 22 b). The alunite-bearing advanced argillic type comprised 58.6 % of drill hole intervals, whereas the potassic type 0.1 % and sericitic-potassic 1.4 % (Table 4). The advanced argillic overprint has strongly affected the copper distribution relative to alteration types (Fig. 23). Rather than the rounded to oval pattern of Cu > 0.5 % overlapping the potassic and sericitic fields that is evident in the first case study (Fig. 12b), the Onto Cu field is elongate at very high K/(K + Ca) ratio extending from potassic to advanced argillic with the highest density of Cu > 0.5 % in the alunite-rich advanced argillic type. Burrows et al (2020) reports that the bulk of the copper mineralisation is hosted in rocks with a mineral composition of 50–60 % quartz, 5–15 % alunite, 10–25 % pyrite and up to 5 % pyrophyllite, dickite and kaolinite. A second smaller concentration of Cu > 0.5 % plots near the origin (Fig. 23), suggesting this relates to propylitic alteration and mineralisation in a mafic rock, most probably the Early Andesites of Burrows et al (2020), which flank the main mineralising porphyrys. The Cu-Au plots (Fig. 24a, b) demonstrate the significance of the alunite-bearing advance argillic event at Onto, where samples with greater than 0.5 % Cu and 0.2 g/t Au dominate the plot of the alunite-rich advanced argillic type, whereas the majority of samples in the pyrophyllite-rich and alunite-poor type rarely reach above 0.1 % Cu and 0.1 g/t Au (see also Table 4).

8. Converting alteration type to bulk mineralogy

The major mineral assemblages that make up any given alteration type in a porphyry copper deposit vary considerably and do not correspond precisely to the alteration boundaries determined in the alteration diagrams discussed above. For example as will be demonstrated, up to 15 wt% white-mica may be found in the potassic alteration field, or up to 10 wt% K-feldspar in the propylitic field.

Bulk mineral variations across the K/(K + Al) vs K/(K + Ca) alteration diagram can be estimated from the major element geochemistry using the MINSQ computer program of Herrmann and Berry (2002). MINSQ is a spreadsheet adaptation of the least squares method that utilizes the Solver tool in Microsoft Excel to quantitatively estimate the proportions of constituent minerals in rocks from whole rock lithogeochemical data. It is simple to use and easily and interactively adaptable to known mineral or normative assemblages. The structure facilitates input of actual mineral chemical analyses for individual rock

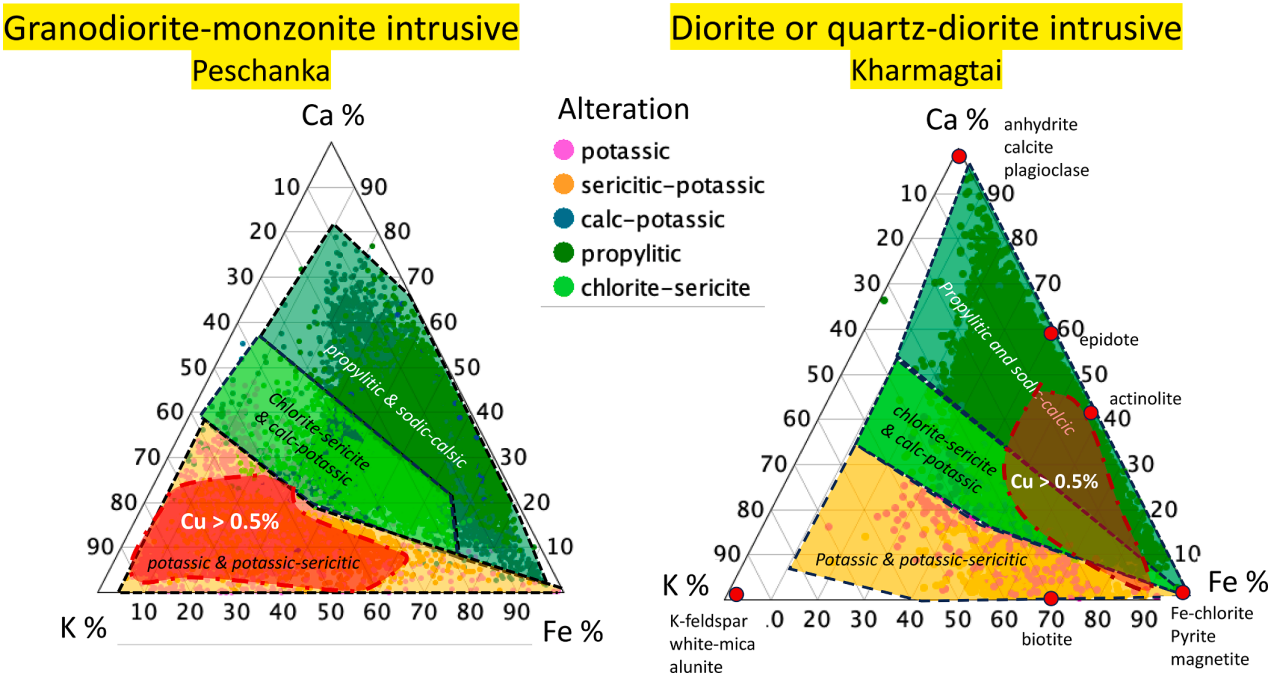

Fig. 19. A) ca-k-fe triangular diagram for all assay data from the peschanka, granodiorite-monzonite porphyry copper deposit. the alteration classification, which defines the boundaries in this diagram are transferred fromFig. 10. Highest density of samples > 0.5 % Cu, shaded red in the potassic and potassic-sericitic field. B) Ca-K-Fe triangular diagram for all assay data from the Kharmagtai, diorite porphyry copper deposit. Alteration classification from Fig. 17b. Highest density of samples > 0.5 % Cu, shaded red in the sodic-calcic and chlorite-sericite fields..

samples (Herrman and Berry, 2002) to produce mineral percentages. The method has been successfully used in a previous study of porphyry copper alteration mineralogy and zoning at the Productora porphyry breccia-pipe deposit, Chile (Escolme et al., 2019).

Here I have applied the MINSQ approach to the Peschanka PCD dataset, and the results are presented in Fig. 25 (a to d). Estimated K-feldspar concentrations calculated by the MINSQ method are highest in the potassic alteration field (Fig. 25a). Maximum K-feldspar concentration reaches 20 to 25 wt% trending diagonally across the potassic field, overlapping through the sericitic-potassic field into the propylitic and the calc-potassic field from 0 to 12 wt% K-feldspar. White-mica reaches 40 to 45 wt% at the top of the sericitic-potassic field and steadily decreases downwards with decreasing K/(K + Ca) ratio to less than 5 wt% in the overlap field (Fig. 25b). White-mica overlaps extensively throughout the potassic field where Cu grades are best developed, and the top parts of the chlorite-sericite and advanced argillic fields. It is noteworthy that the highest concentration of samples with > 0.5 % Cu corresponds with samples showing maximum variation in K-felspar to white-mica ratio from approximately 2 to 1 to 1 to 40. Estimated quartz concentrations are a minimum in the centre of the alteration diagram (Fig. 25c), around 30 to 40 wt%, and increase outwards, such that the calc-potassic field is very siliceous, varying from 65 to over 90 wt% quartz. Na-Ca plagioclase, including albite, shows roughly the reverse pattern to quartz with the greatest concentrations (30——40 wt% plagioclase) in the centre of the diagram and decreasing to the margins. The 10–30 % plagioclase in the advanced argillic alteration field is probably incorrect as most of the samples classified as advanced argillic alteration at Peschanka occurs in near surface drill samples related to surface oxidation, causing feldspar replacement by clays. As expected, chlorite and epidote are at a maximum in the left bottom corner where they reach 20 to 25 wt%, and extend throughout the propylitic field with overlap into adjacent fields from 1 to 10 wt% combined.

The relative alteration mineral concentrations across the K/(K + Al) vs K/(K + Ca) diagram indicate that the presence of a key mineral, such as K-feldspar, is not sufficient to classify the alteration as potassic. The propylitic alteration field has up to 10 % K-feldspar in the upper right side (Fig. 25a), but the mineral assemblage also includes 20–30 % plagioclase, 10–20 % epidote and 10–15 % chlorite. In the approach described here, based on geochemistry and mineralogy, it is the full mineral assemblage that defines the alteration type, not the presence or absence of a key mineral. But this depends if the mineral concerned is part of a single assemblage or is overprinted. In mapping alteration, sillitoe (pers comm) states that the predominant assemblage dictates the alteration type designation. If two assemblages occur together in roughly equal proportions, then it is mapped as a hybrid alteration, say potassic-sericitic. This would, I think, be common practice (Sillitoe, pers comm).

A typical downhole plot from Peschanka of estimated mineralogy is shown for drill hole DHP17-T14 in Fig. 26. This hole intersects a zone of potassic alteration overprinted by sericitic alteration from 35 to 205 m. In the interval of best Cu grades (75 to 135 m), K-feldspar varies from 10 to 40 %, white-mica from 15 to 27 %, chlorite from 5 to 10 % and biotite from 0 to 2 %. Surprisingly there is no relationship between Cu sulfide and K-feldspar or biotite concentrations throughout the drill hole, but weak positive relationships between Cu sulfides and white-mica and Cu sulfides and quartz (Fig. 27). However, this may be complicated by how much of the K-feldspar and biotite is magmatic rather than hydrothermal. The conventional explanation for the relationships in Fig. 27 is that the Cu minerals are inherited from a pre-existing potassic facies now overprinted by chlorite and white-mica. The weak correlation with quartz is expected as most of the Cu-sulfides are in quartz veins, but the correlation of Cu with white-mica could be explained by another explanation. A possibly related feature is that although biotite is present up to 10 % in weakly mineralised samples, it drops to near zero in samples with Cu-sulfide concentrations greater than 2 %, most likely due to replacement of biotite by chlorite and white-mica. These relationships

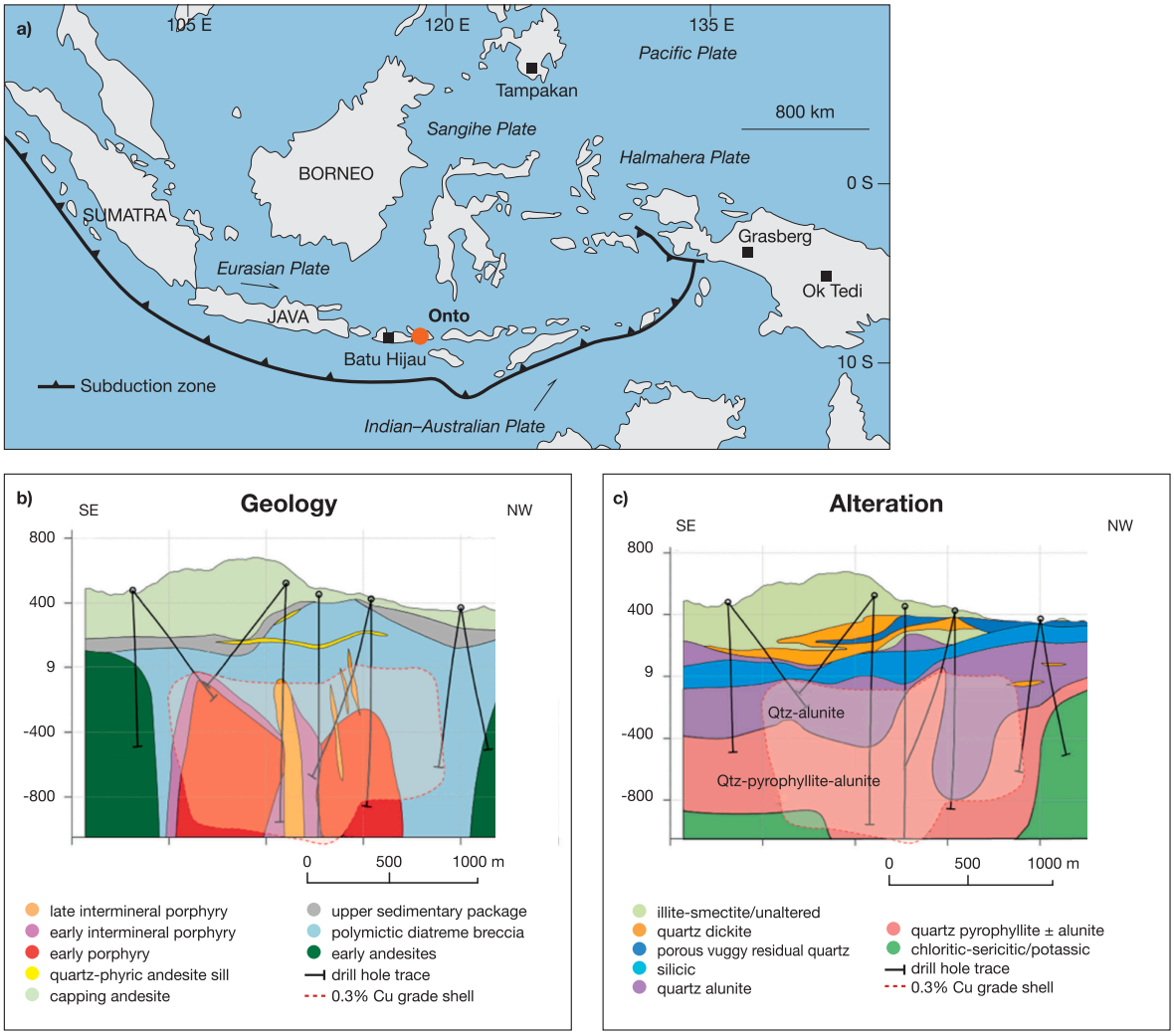

Fig. 20. A) locality diagram for onto porphyry cu-au deposit, showing location of other porphyry deposits in indonesia. b) onto geology cross-section (Burrows et al., 2020), c) Alteration types on the same section as b (Burrows et al., 2020).

suggest that the replacement of K-feldspar by white mica, and biotite by chlorite plus white-mica, may be directly related to Cu-sulfide deposition at Peschanka.

$$\underset{K-feldspar}{3KAlSi_3O_8} + 2H^+ + 12H_2O \rightarrow \underset{white-mica}{KAl_2(AlSi_3O_{10})(OH)_2} + 6H_4SiO_4 + 2K^+.$$

$$\underset{biotite}{5K(Mg,Fe)_3AlSi_3O_{10}(OH)_2} + 24H^+ + 6H2O \rightarrow \underset{chlorite}{\{(Mg,Fe)_5Al\}(Si_3Al)O_{10}(OH)_8} + \underset{white-mica}{KAl_2(AlSi_3O_{10})(OH)_2} + 4K^+ + 10(Mg,Fe)^{2+} + 9H_4SiO_4$$

These replacement reactions involve consumption of hydrogen ions, leading to increasing pH and thus provide one potential mechanism for deposition of copper sulfides (Hemley and Hunt, 1992). There are many other ways copper sulfides may be deposited such as P and T variations, hydrofracturing, phase separation and reduction, but none of these explain the relationship of sericitic alteration to copper sulfide deposition.

The MINSQ method has also been employed to better understand the relationship between Cu-Au grades and alteration in the diorite-hosted porphyry at the Kharmagtai deposit (Fig. 28 a to d). Estimated K-feldspar reaches over 20 wt% in the potassic field (compared with ~ 9 wt% in least altered diorites) and shows maximum concentration along the boundary between potassic and calc-potassic fields. It overlaps the sericitic field and extends into the chlorite-sericite field at 5 to 10 wt% K-feldspar (Fig. 28a). Biotite is largely restricted to the potassic field reaching over 30 wt% close to the middle of the field (Fig. 28b). White-mica is concentrated at 5 to 30 wt% in the upper half of the alteration plot (Fig. 28c), whereas pyrophyllite (or kaolinite) occurs overlapping the left side of the white-mica distribution at lower K/(K + Al) ratios confines to the advanced argillic field (Fig. 28c). A broad field of chlorite at 5 to 15 wt% occurs over the centre of the alteration diagram overlapping all alteration types, whereas epidote concentrates at the bottom of the diagram principally in the propylitic field (Fig. 28d). The

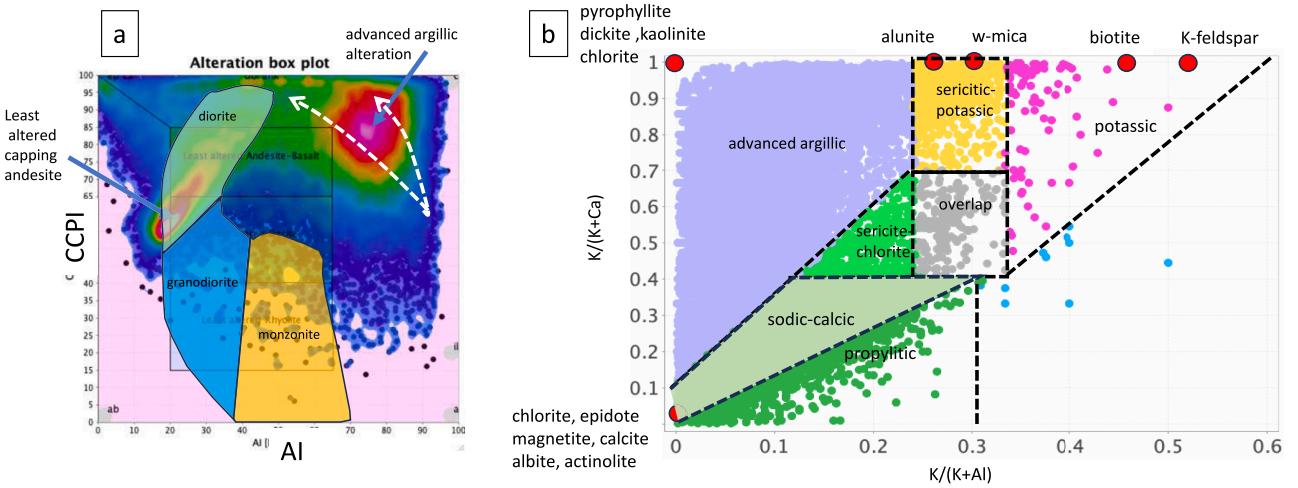

Fig. 21. A) onto drill geochemical database plotted on the ai vs ccpi density diagram. the highest density of samples plots well to the right of the least altered diorite field. this suggests the intensity of alteration in the porphyry is very high and prevents any interpretation of the least altered mineralised porphyry. a small field of high sample density on the lhs of the diagram most probably represents the capping andesite with little or no alteration. b) onto k/(k + Al) vs K/(K + Ca) diagram showing the porphyry alteration type before the alunite-rich advanced argillic event. Compare this with Fig. 22b which gives the alteration type after the alunite-bearing advanced argillic event.

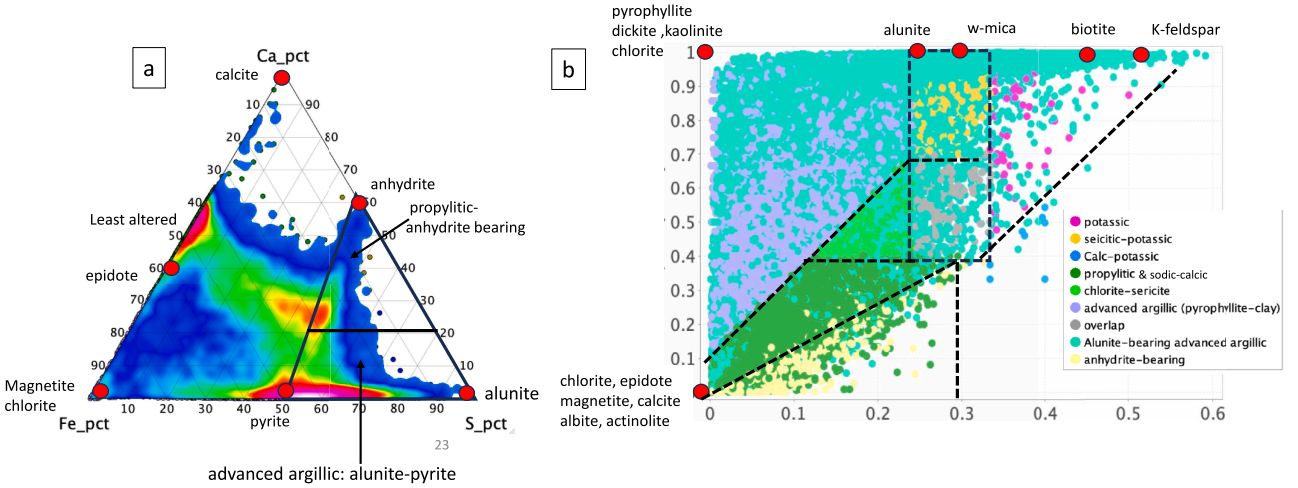

Fig. 22. A) onto ca-fe-s triangular sample density plot highlighting the position of alunite, anhydrite and pyrite. this diagram, afterHalley (2021), is a simple way to identify alunite in the advanced argillic alteration. b) K/(K + Al) vs K/(K + Ca) diagram showing the distribution of the overprinting alunite-rich advanced argillic alteration in relation the other alteration types at Onto.

Table 4
Onto mean Cu and Au concentration for each alteration type determined from Fig. 22b.

Alteration facies	Cu %	Au g/t	Nos. samples	Percentage of samples
Potassic	0.41	0.31	78	0.1
Sericitic-potassic	0.44	0.33	860	1.4
propylitic	0.09	0.07	16,782	26.8
Chlorite-sericite	0.28	0.14	371	0.6
Advanced argillic alunite	0.62	0.34	36,629	58.6
Advanced argillic pyrophyllite	0.13	0.1	7593	12.1
Overlap	0.3	0.19	205	0.3

distribution of high −grade samples of Cu and Au does not exhibit any relationship to K-feldspar, biotite, white-mica or pyrophyllite distribution, in-fact they are mutually exclusive of Cu across the diagram. On the other hand, estimated tourmaline concentration (5 to over 10 wt%), which overlaps the propylitic and chlorite-sericite fields, roughly corresponds to the highest Cu and Au grades where samples with > 1 ppm Au and > 1.5 % Cu are concentrated (Fig. 28a). Kirwin et al, (2005) reports that tourmaline, occurs in mineralized tourmaline breccias and veins commonly throughout the mineralized diorite porphyries at Kharmagtai. It appears that the alteration that correlates well with the best Cu-Au grades at Kharmagtai is albitisation of plagiocase in the sodic-calcic field and tourmaline alteration (5 to 15 wt%) overprinting the sodic-calcic and sericite-chlorite fields (Fig. 28b). Of possible significance also is the fact that the best Cu-Au grades coincide with the overlap of chlorite and epidote concentrations, although the assemblages with maximum chlorite or epidote are only weakly mineralised.

Alunite and pyrophyllite concentrations have been contoured over

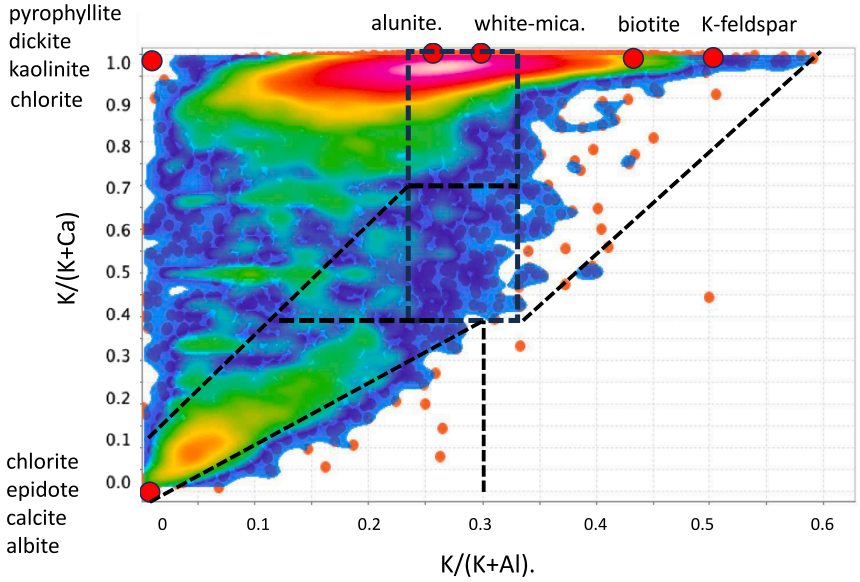

Fig. 23. Density plot of samples > 0.5 % Cu on the K/(K + Al) vs K/(K + Ca) diagram for the Onto porphyry copper–gold deposit.

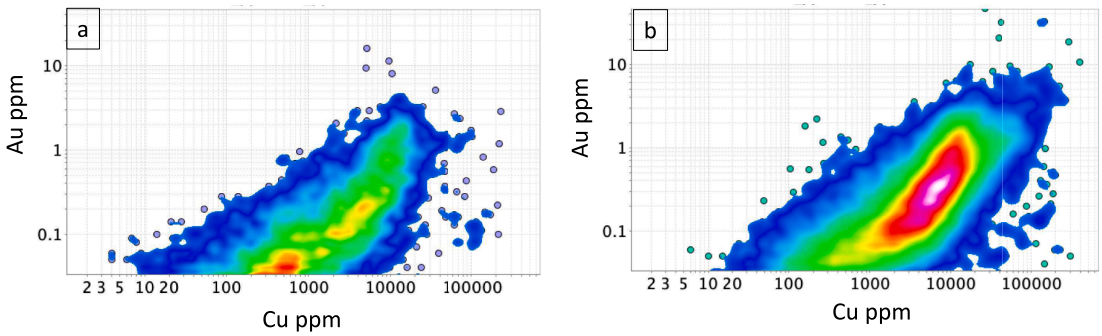

Fig. 24. Onto Cu-Au plots for a) pyrophyllite-rich advance argillic alteration lacking alunite, and b) alunite-bearing advanced argillic alteration, demonstrating that the latter alteration type has a high density of samples above 0.5 % Cu and 0.2 g/t Au compared with the former (Table 4).

the K/(K + Al) vs K/(K + Ca) diagram for the Onto deposit (Fig. 29a to d), where they are compared to quartz and covellite concentrations. Due to the extensive advanced argillic alteration overprint at Onto the maximum concentration of alunite (10 to 20 wt%) is in the upper parts of the potassic and sericitic field, decreasing away from this area. Less than 1 wt% alunite is estimated for the bottom half of the diagram (Fig. 29a), although the presence of Na-bearing alunite (natroalunite) cannot be estimated and may be present at low K/K + Al ratios. Quartz concentration is elevated to over 70 wt% in the upper right of the alteration diagram for Onto, reaching over 80 % in the far right at maximum K/K + Ca) and K/(K + Al) ratios (Fig. 29b). Pyrophyllite is over 40 wt% along the left upper side of the diagram (Fig. 29b), where alunite is < 1 wt%, and generally decreases with increasing K/(K + Al) ratio. Covellite concentrations above 1.0 wt%, occur with the very siliceous alteration type of > 70 wt% quartz (Fig. 29d), most likely corresponding with the highly siliceous vuggy quartz zone in Onto with the highest covellite grades, reported by Burrows et al (2020). This high-grade Cu-Au field also has bulk concentrations of alunite from 5 to 15 wt% (Fig. 29a). The very different pattern of pyrophyllite distribution compared with quartz-alunite poses the question of whether quartz-alunite alteration, that correlates well with covellite concentration at Onto, was a separate later event from the pyrophyllite-bearing advanced argillic alteration. Petrographic evidence of overprinting would be required to justify this interpretation.

9. Conclusions, limitations and future research

9.1. Conclusions

The recommended steps developed here, as a first pass, to determine porphyry copper alteration type using a major element drill hole database are:

Determine the original least altered porphyry composition(s) by using the AI vs CCPI plot in combination with the Gard database.
Try the molar K/Al vs Na/Al plot to discriminate some of the alteration types
Check for occurrence of alunite and anhydrite +/- gypsum using the Ca-Fe-S triangular plot.
Plot the samples on a K/(K + Ca) vs K/(K + Al) diagram to finalise the discrimination of alteration types
Plot all data with Cu > 0.5 % (and Au > 0.5 ppm) on the alteration plot (4 above), as a density plot, to evaluate the relationship between Cu and Au grades and alteration type.
When bulk mineral assemblages are required, as say in geometallurgical studies, the major element dataset can be treated with the MINSQ method and plotted back to the K/(K + Al) vs K/(K + Ca) plot, so that alteration type, bulk mineralogy and ore grades can be assessed.

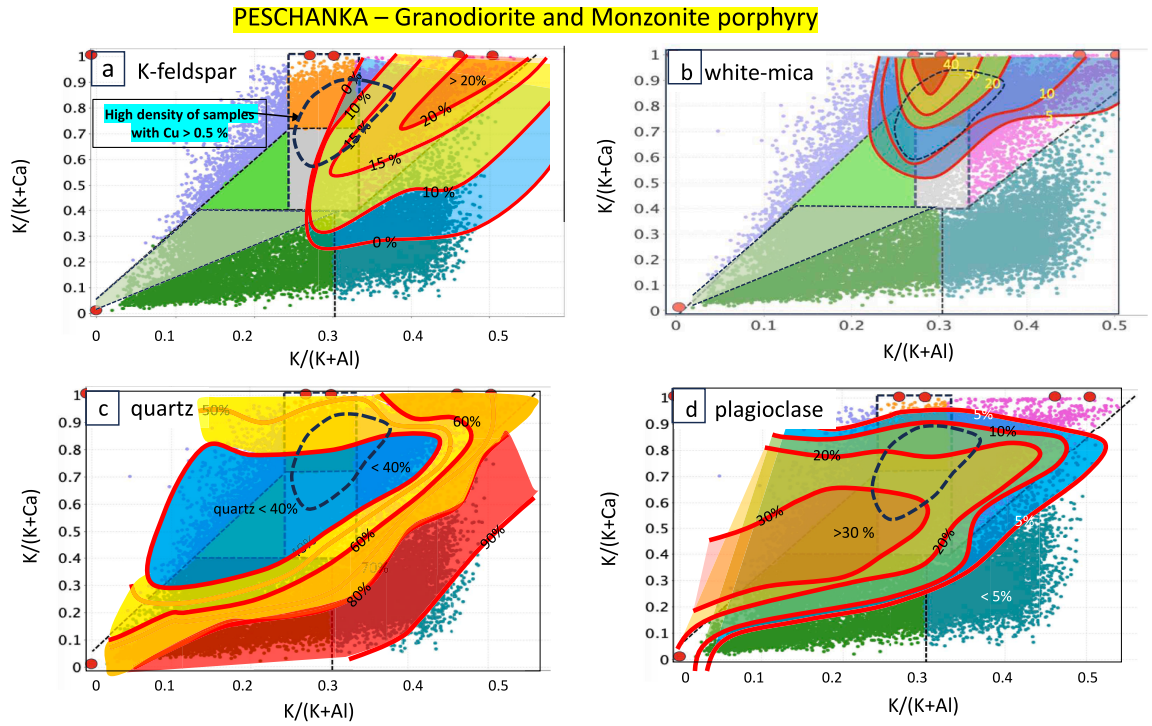

Fig. 25. Peschanka: Contours of alteration mineral concentrations estimated by MINSQ plotted over the porphyry copper alteration type diagram; a) K-feldspar, b) white-mica, c) quartz and d) plagioclase. Alteration type colours and fields as for Fig. 10.

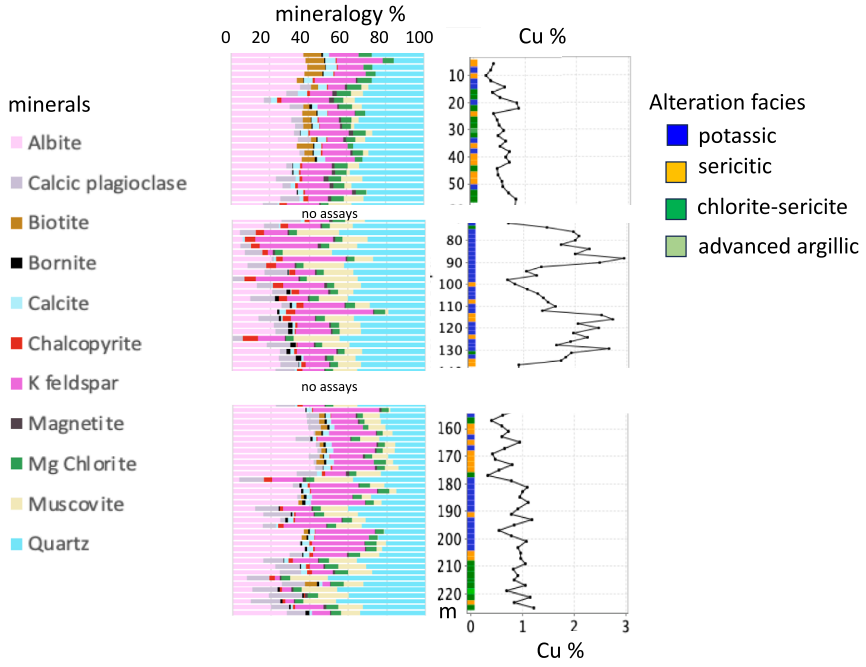

Fig. 26. Peschanka down hole DHP17-T14 mineral distribution plot determined from MINSQ with Cu % grades and alteration type from Fig. 10.

The alteration type diagram [K/(K + Al) vs K/(K + Ca)] for porphyry copper deposits developed from this study is shown in Fig. 30, indicating the most common minerals found in each field of the diagram, determined from the mineral nodes, the MINSQ estimations (Figs. 25, 28, 29) and the summary of alteration types by Seedorff et al. (2005).

The most significant conclusion from this study, supports previous conclusions by Hollister (1974, 1991), that the composition of the host rock porphyries is fundamental in controlling the nature of the alteration type, mineral distribution and their relationship to copper and gold grades (compare Fig. 12b, 18a, 19 and 23). As mentioned earlier, dioritic and quartz dioritic compositions constitute less than around 13 % of porphyry copper deposits in north and South America porphyry

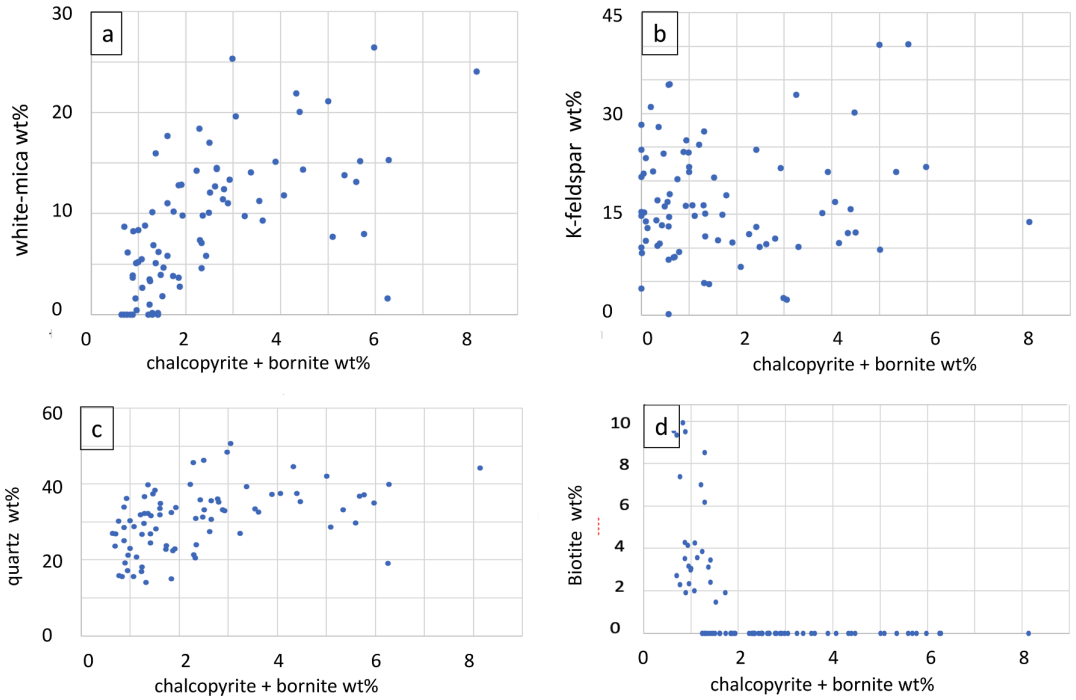

Fig. 27. Peschanka, alteration mineral concentration data plotted against copper sulfide concentration for DHP17-T14. Demonstrates a weak to moderate correlation between copper sulfide concentration and white-mica concentration and between copper sulfide concentration and quartz concentration. No significant correlation exists between Cu −sulfides and K-feldspar or Cu −sulfides and biotite.

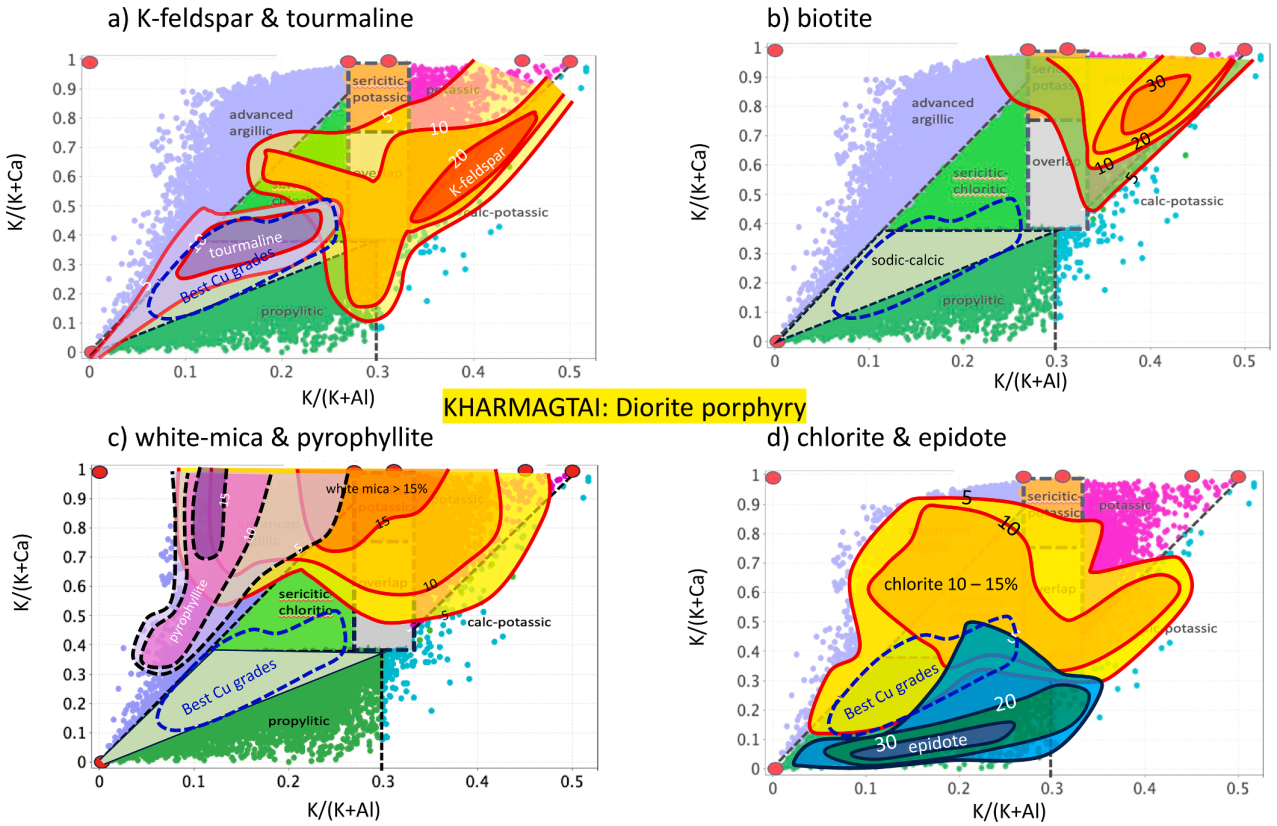

Fig. 28. Kharmagtai: Contours of alteration mineral concentrations estimated by MINSQ plotted over the PCD alteration type diagram; a) K-feldspar and tourmaline b) biotite, c) white-mica and pyrophyllite and d) chlorite and epidote. Alteration colours same as Fig. 17b.

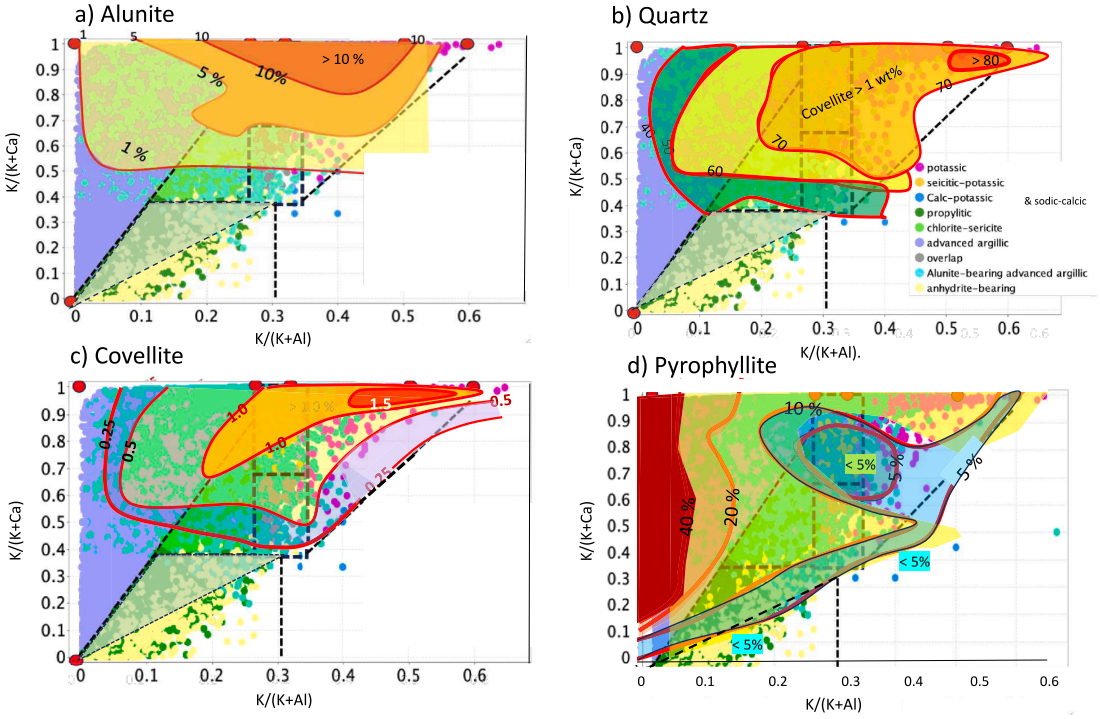

Fig. 29. Onto: Contours of alteration mineral concentrations estimated by MINSQ plotted over the PCD alteration diagram; a) alunite, b) quartz, c) covellite and d) pyrophyllite.

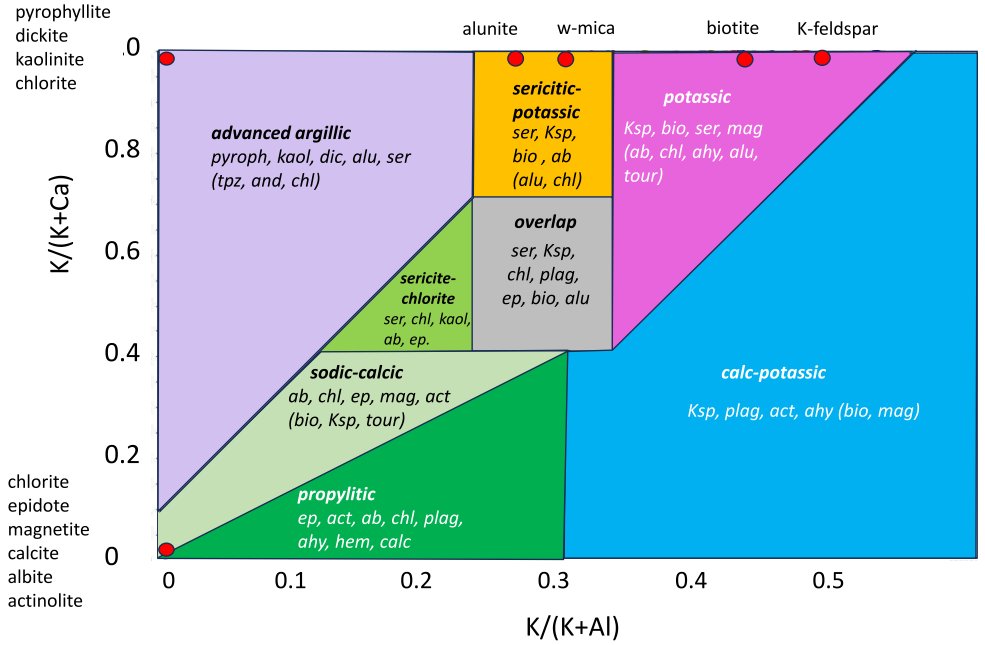

Fig. 30. The alteration diagram for porphyry copper deposits derived from this study with the common mineralogy of each type. The minerals in brackets are minor constituents. Abreviations: Ksp-K-feldspar, bio-biotite, ser-sericite, chl-chlorite, ab-albite, plag-plagioclase, act-actinolite, ep-epidote, pyroph-pyrophyllite, alu-alunite, kaol-kaolinite, dic-dickite, mag-magnetite, tpz-topaz, and-andalusite, calc-calcite, tour-tourmaline, hem-hematite.

provinces, with the remaining 87 % related to granodiorite, monzonite and quartz-monzonite compositions. Some porphyry districts have a range of intrusions from diorite to monzonite, but it is commonly the granodiorite to monzonites that are related to significant copper +/- molybdenum mineralization (e.g., Morenci in SW USA and El Abra in S. American Andes), whereas the dioritic intrusions tend to host enriched gold-copper mineralization (e.g., Cerro Casale, Lobo, Dizon, Far South East and Panguna; Sillitoe, 2000). The monzonite and granodiorite porphyries with moderate to high primary potassium content (Fig. 31b) commonly have their best copper grades in the potassic alteration, or

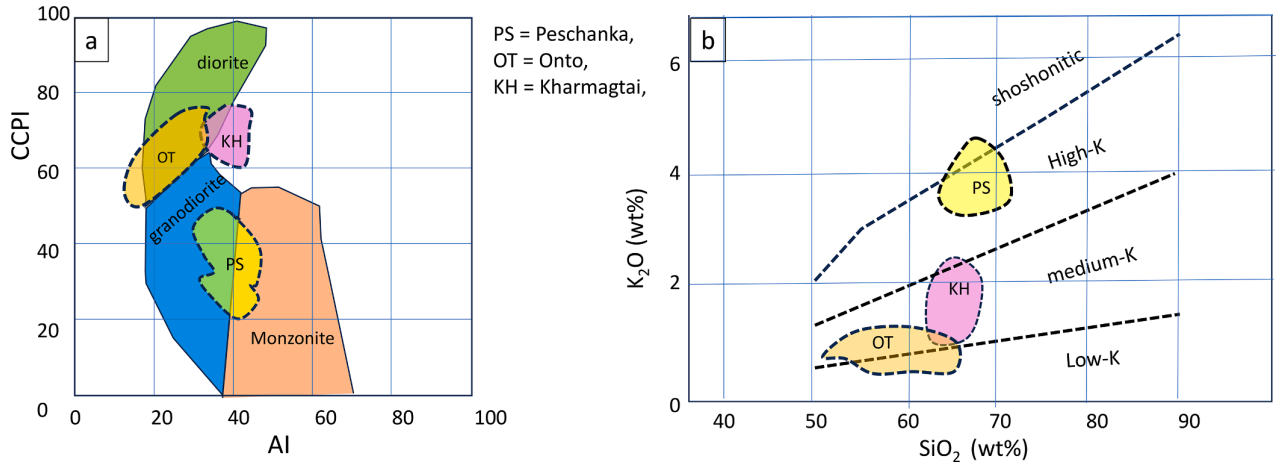

Fig. 31. Least altered porphyry compositions in the three case studies plotted on a) AI vs CCPI diagram, and b) SiO_2 vs K_2O diagram.

where potassic is overprinted by sericitic or chlorite-sericite alteration. In contrast the low-K diorite porphyry investigated here (Kharmagtai) has their best copper and gold concentrated in the sodic-calcic alteration (Fig. 18a, 19), where it is overprinted by white-mica or chlorite-sericite alteration. Albitisation of plagiclase is a dominant process in the sodic-calcic Cu-Au mineralised core of diorite porphyries. Even though the diorite porphyries may have inner zones with biotite alteration, the overall chemistry and mineralogy of the copper–gold zones indicates sodic-calcic alteration of porphyry with abundant albite, chlorite, and plagioclase +/- epidote, actinolite, biotite and commonly nil or very minor concentrations of K-feldspar. Whether most diorite and quartz diorite-hosted porphyry copper–gold deposits show this relationship of sodic-calcic rather than potassic alteration will require further research, but previous studies by (Hollister, 1974, 1991) suggest his proposal of a separate descriptive model for diorite-based porphyries may be necessary.

A second conclusion is that the presence of potassic alteration (K-feldspar, biotite), by itself, may not indicate higher grade copper mineralization. The overprint of potassic by sericitic or chlorite-sericite alteration appears to be a more important Cu-mineralizing event in the Peschanka case study and this may be an important feature of other granodiorite based porphyries.

A third conclusion, based on the Onto case study, is that intense advanced argillic alteration may move copper from the potassic and sericitic alteration into the advanced argillic alteration. Also, the data at Onto suggests the quartz-alunite alteration, which is more closely associated with covellite, may be a separate event to the pyrophyllite-rich advanced argillic alteration.

A further conclusion is that although the alteration boundaries on the plots are relatively fixed, or vary only by a few percent, for all the porphyry deposits examined, the actual bulk mineralogy in each alteration field shows considerable change of up to 50 %, and is slightly different for each example. This relates to two factors 1) the composition of the primary causative porphyry and the surrounding country rocks, and 2) the degree of alteration overprinting; sericitic overprinting in the case of Peschanka, and advanced argillic overprinting in the case of Onto.

The final conclusion is that the methodology presented here is a first pass approach that needs to complement and be refined by core logging and other available techniques such as SWIR analysis, petrography and XRD analysis where appropriate. Some of the assumptions and conclusions from this research may prove to be wrong when more case studies are investigated.

9.2. *Limitations and future research*

Geoscientists who apply this approach to alteration mapping need to be fully aware of the limitations of the method. This is not a stand-alone method, but should be used in conjunction with visual logging, petrology and other mineral mapping techniques. The most important limitations are discussed below.

This work is based on only three case studies, however a further four case studies were undertaken which support these conclusions, but are not available for publication due to confidentiality. Two studies on diorite-hosted porphyry copper deposits and two further studies on granodiorite-monzonite-hosted porphyries support the alteration and copper distribution patterns recorded at Kharmagtai (diorite-hosted) and Peschanka (monzonite-hosted). More published in-depth studies of alteration geochemistry from other porphyry copper deposits in other districts will help to make the method and conclusions more robust.

This approach suffers from the fact that it is challenging, if not impossible, to identify overprinting alteration events from the geochemistry alone. This weakness is particularly an issue if the samples are bulked over several meters, such that minor to moderate overprinting is completely lost in the bulked assay data.

It is only possible to distinguish the main seven alteration types using this approach; potassic, sericitic-potassic, chlorite-sericite, sodic-calcic, propylitic, advanced argillic and calc-potassic. Quartz-rich sub-type such as vuggy silica, quartz-dickite, quartz-alunite and quartz-pyrophyllite cannot be easily separated. However further development of the MINSQ conversion to bulk mineralogy will assist the distinction of such other alteration types.

The approach described here recognises alteration type defined by the full geochemical-mineralogical components in the rock, not the presence of one key mineral in say veinlet alteration or selective pervasive alteration. For example, key alteration minerals like K-feldspar or epidote may be present at around 5 % in an altered rock in veinlets or patches, but if the assemblage is dominated by chlorite and white-mica, then the rock plots in the sericite-chlorite field, not the potassic or propylitic fields.

The results presented here are scale dependent; we have used a scale of whole rock analysis of split core every 1 to 3 m down the drill hole. If the sampling interval was say, 0.2 m or bulked over 20 m the results may well be different.

Another important limitation is that the boundaries developed for the various alteration plots are not precisely fixed in place. They vary according to the composition of the host porphyry intrusions and also due to chemical variations in the composition of minerals, particularly white mica which displays considerable variation in K/Al, Si/Al and (Fe

+ Mg/Al) ratios. Consequently, the boundary between the sericitic-potassic and potassic fields can change, in terms of K/(K + Al) ratio from one porphyry to the next. This issue requires further study.

The exact nature of overprinting alteration assemblages is important to resolve. This should involve textural and mineralogical studies at the core logging scale and thin section scale, integrated with this geochemical approach. How many types of overprinting events exist and are they systematic across most porphyries or dependent on the primary least altered composition of the cauastive porphyry?

It is not possible to determine, using this approach, the difference between high primary potassium in a porphyry intrusion from potassic alteration. In addition to petroraphy, are there simple geochemical means of distinguishing primary potassium in a high K-monzonite from addition of hydrothermal potassium associated with potassic alteration?

It has proved to be possible to use pXRF analyses on drill chips, in addition to lab-based multi-element analyses to apply this methodology. This approach has been successfully tested in the field and greatly assists and speeds-up alteration recognition during an RC drilling program. However, the lack of the ability to analyse Na in most pXRF units reduces the use of the AI-CCPI and K/Al vs Na/Al (molar) plots and only the K/(K + Ca) vs K/(K + Al) alteration plot is possible. In addition, care needs to be taken to ensure that aluminium and magnesium analyses are sufficiently accurate, because Al and Mg are low atomic number elements that commonly give poor results if the pXRF is not precisely and continually calibrated by the use of standards.

The MINSQ conversion from multielement geochemistry to mineralogy is appropriate for major mineral concentration estimates but is not recommended for concentrations of minor phases such as magnetite, apatite and rutile, where Fe, Ca and Ti are also present in other major mineral phases. It is also less reliable in distinguishing between bornite and chalcopyrite concentrations. It is critical, therefore, that petrology is undertaken to determine the mineral assemblages in each alteration zone, before applying the MINSQ conversion. This approach does not determine the mineral assemblage, but only estimates the concentration of each mineral in the assemblage.

Declaration of competing interest

The authors declare that they have no known competing financial interests or personal relationships that could have appeared to influence the work reported in this paper.

Acknowledgements

I had considerable help from many colleges, as porphyry deposits have not been my principal interest over my 30 years of ore deposit research. Firstly, the pionerring research of countless porphyry copper specialists, especially David Lowell, Dick Sillitoe, Vic Hollister, Spense Titley and Eric Seedorff have beern guiding lights for this contribution. Scott Halley's recent work on mineralogy and alteration associated with porphyry Cu deposits was of great assistance and his help along the way was critical to me completing this project. Also, the help of Imants Kavalieris and Khashgerel Bat-Erdene in getting approvals to use porphyry copper data sets and giving me encouragement to continue was of immense importance. Tony Crawford gave advise on the petrology of alteration and helped in discussions over a few drinks, red for me and coca cola for him. Ron Berry guided me through the use of the MINSQ program which was critical to being able to more accurately determine variations in bulk mineralogy across the alteration type of a porphyry copper deposit. Robert Scott assisted greatly by upgrading the MINSQ program so that batches of analyses could be converted to mineralogy at a faster rate. Listening to David Cooke and his PhD students give many talks on porphyry deposits over more than 20 years laid a great foundation for this project. Mike Baker provided some key photos of porphyry alteration in drill cores. Tristan Wells generously provided porphyry geochemistry data sets from his PhD and publications. The six reviewers, Dave Burrows, Thomas Bissig, Farhad Bouzari, Fedferico Cernushi, plus two anominous reviewers in addition to Dick Sillitoe and Louise Corriveau gave invaluable comments to improve the quality of the manuscript. Approvals from the various exploration companies to use their data sets in this paper is very much appreciated, including Vale, Baimskoye and Xanadu Mines.

Data availability

The data that has been used is confidential.

References

Ahmed, A.D., 2019. Epidote and chlorite mineral chemistry from the Yerington porphyry copper district, USA: genetic and exploration implications (Doctoral dissertation, University of Tasmania), 349 p.

Bachmann, K., Gutzmer, J. and Mac Fjellerad Persson, N.J., 2013. Alteration in the area of the Kristineberg VHMS deposit, Skellefte district, Sweden. In 12th Biennial SGA Meeting on Mineral Deposit Research for a High-Tech World Conference Location Uppsala, SWEDEN (p. 498). SGU-SVERIGES GEOLOGISKA UNDERSOKNING-GEOLOGY SURVEY SWEDEN Location UPPSALA.

Burrows, D.R., Rennison, M., Burt, D., Davies, R., 2020. The Onto Cu-Au discovery, eastern Sumbawa, Indonesia: A large, middle Pleistocene lithocap-hosted high-sulfidation covellite-pyrite porphyry deposit. Econ. Geol. 115, 1385–1412.

Cathles, L.M., Shannon, R., 2007. How potassium silicate alteration suggests the formation of porphyry ore deposits begins with the nearly explosive but barren expulsion of large volumes of magmatic water. Earth Planet. Sci. Lett. 262, 92–108.

Chitalin, A.F., Formichev, E., Usenko, V., Agapitov D. and Shtengelow, A., 2012, Structural model of Peschanka porphyry Cu-Au-Mo deposit, Western Chukotka, Russia: Structural Geology and Resources, Conference paper, p. 21-27.

Cooke, D.R., Baker, M., Hollings, P., Sweet, G., Chang, Z., Danyushevsky, L., Gilbert, S., Zhou, T., White, N.C., Gemmell, J.B. and Inglis, S., 2014, New advances in detecting the distal geochemical footprints of porphyry systems—epidote mineral chemistry as a tool for vectoring and fertility assessments, In: Kelley , Karen D., and Golden, Howard C., (eds.) Building Exploration Capability for the 21st Century. SEG Special Publication, 18. Society of Economic Geologists, Boulder, CO, USA, p. 127-152.

Cook, D.R., Agnew, P., Hollings, P., Baker, M., Chang, Z., Wilkinson, J.J., Ahmed, A., White, N.C., Zhang, L., Thompson, J., Gemmell, J.B., 2000. Recent advances in the application of mineral chemistry to exploration for porphyry copper–gold–molybdenum deposits: detecting the geochemical fingerprints and footprints of hypogene mineralization and alteration, Geochemistry: Exploration. Environment, Analysis 20, 176–188.

Creasey, S.C., 1959. Some phase relations in the hydrothermally altered rocks of porphyry copper deposits. Econ. Geol. 54, 351–373.

Eastoe, C.J., Solomon, M., Walshe, J.L., 1987. District-scale alteration associated with massive sulfide deposits in the Mount Read Volcanics, western Tasmania. Econ. Geol. 82, 1239–1258.

Escolme, A., Berry, R.F., Hunt, J., Halley, S., Potma, W., 2019. Predictive models of mineralogy from whole-rock assay data: Case study from the Productora Cu-Au-Mo deposit, Chile. Econ. Geol. 114, 1513–1542.

Franklin, J.M., Lydon, J.W. and Sangster, D.F., 1981, Volcanic-associated massive sulfide deposits. 75th Anniversary volume: Economic Geology, p. .485-627.

Gard, M., Hasterok, D., Halpin, J.A., 2019. Global whole-rock geochemical database compilation. Earth Syst. Sci. Data 11, 1553–1566.

Gifkins, C.C., Herrmann, W., Large, R.R., 2005. Altered volcanic rocks; a guide to description and alteration: Centre for Ore Deposit Research. University of Tasmania, p. 156.

Gisbert, G., Tornos, F., Losantos, E., Pons, J.M., Videira, J.C., 2021. Vectors to ore in replacive volcanogenic massive sulfide (VMS) deposits of the northern Iberian Pyrite Belt: mineral zoning, whole rock geochemistry, and application of portable X-ray fluorescence. Solid Earth 12, 1931–1966.

Guilbert, J.M., Park Jr, C.F., 2007. The geology of ore deposits. Waveland Press, p. 985.

Gustafson, L.B., Hunt, J.P., 1975. The porphyry copper deposit at El Salvador, Chile. Econ. Geol. 70, 857–912.

Halley, S., 2020. Mapping magmatic and hydrothermal processes from routine exploration geochemical analyses. Econ. Geol. 115, 489–503.

Halley, S., 2021, Porphyry Copper Workshop; Part 2 Alteration Geochemistry: Workshop presented to CODES masters course, 2021, 28p. https://www.scotthalley.com.au/tutorials.

Hedenquist, J.W., Watanabe, Y., Arribas, A., 2020. Hypogene alunite from the El Salvador district, Chile, indicates potential for a blind porphyry copper center. Econ. Geol. 115, 231–239.

Hemley, J.J., Hunt, J.P., 1992. Hydrothermal Ore-Forming Processes in the Light of Studies in Rock-Buffered Systems I:I. Some General Geologic Applications. Economic Geology 87, 23–43.

Herrmann, W., Berry, R.F., 2002. MINSQ–a least squares spreadsheet method for calculating mineral proportions from whole rock major element analyses: Geochemistry: Exploration. Environment, Analysis 4, 361–368.

Hollister, V.F., 1974. Regional characteristics of porphyry copper deposits of South America. Transactions of SME-AIME 256, 45–53.

Hollister, V.F., 1978. Geology of the Porphyry Copper Deposits of the Western Hemisphere: AIME. N. Y. 177–199.

Kirwin, D.J., Wilson, C.C., Turmagnai, D., Wolfe, R., 2005. Exploration history, geology, and mineralisation of the Kharmagtai gold–copper porphyry district, South Gobi region, Mongolia. Geodynamics and Metallogeny of Mongolia with a Special Emphasis on Copper and Gold Deposits: SEG-IAGOD Field Trip 14, 16p.

Krushnisky, A., Mercier-Langevin, P., Ross, P.S., Goutier, J., McNicoll, V., Moore, L., Monecke, T., Jackson, S.E., Yang, Z., Petts, D.C., Pilote, C., 2023. Geology and Controls on Gold Enrichment at the Horne 5 Deposit and Implications for the Architecture of the Gold-Rich Horne Volcanogenic Massive Sulfide Complex, Abitibi Greenstone Belt: Canada. Econ. Geol. 118, 285–318.

Large, R.R., Gemmell, J.B., Paulick, H., Huston, D.L., 2001. The Alteration Box Plot: A Simple Approach to Understanding the Relationship between Alteration Mineralogy and Lithogeochemistry Associated with Volcanic-Hosted Massive Sulfide Deposits. Economic Geology 96, 957–971.

Large, R.R., 1977. Chemical evolution and zonation of massive sulfide deposits in volcanic terrains. Econ. Geol. 72, 549–572.

Leveille, R.A., Stegen, R.J., 2012. 2012, The southwestern North America porphyry copper province, in Geology and Genesis of Major Copper Deposits and Districts of the World. A Tribute to Richard H, Sillitoe.

Lowell, J.D., Guilbert, J.M., 1970. Lateral and vertical alteration-mineralisation zoning in porphyry ore deposits. Econ. Geol. 65, 373–408.

McNulty, B.A., Gemmell, J.B., Davidson, G., Fox, N., 2023. Integrated stratigraphy, lithotype, and U–Pb geochronology of the Myra Falls VHMS deposits, British Columbia, Canada: implications for episodic volcanism and ore deposit formation. Miner. Deposita 58, 307–335.

Meyer, C., Hemley, J.J., 1967. Wall rock alteration. Holt, Rinehart and Winston, In Geochemistry of hydrothermal Ore deposits, pp. 166–235.

Middlemost, E.A., 1994. Naming Materials in the Magma/igneous Rock System. Earth-Science Reviews 37, 215–224.

Mills, H.K., Piercey, S.J., Toole, T., 2016. Geology, alteration, and lithogeochemistry of the Hood volcanogenic massive sulfide (VMS) deposits, Nunavut, Canada. Miner. Deposita 51, 533–556.

Ohmoto, H., 1996, Formation of volcanogenic massive sulfide deposits: The Kuroko perspective: Ore geology reviews, v. 10, p.135-177.

Pacey, A., Wilkinson, J.J., Cooke, D.R., 2020. Chlorite and epidote mineral chemistry in porphyry ore systems: A case study of the North Parkes district, New South Wales, Australia. Economic Geology 115, 701–727.

Pour, A.B., Hashim, M., 2011. Identification of hydrothermal alteration minerals for exploring of porphyry copper deposit using ASTER data. SE Iran: Journal of Asian Earth Sciences 42, 1309–1323.

Rodrigues, S., Esterle, J., 2016. Core scanner technologies – take everything without breaking. APPEA - Oil and Gas Conference and Exhibition. APEA Journal 56, 595–607.

Seedorff, E., Dilles, J.H., Proffett, J.M., Einaudi, M.T., Zurcher, L., Stavast, W.J., Johnson, D.A. and Barton, M.D., 2005, Porphyry deposits: Characteristics and origin of hypogene features: Economic Geology 100th Anniversary volume, p.251-298.

Sharma, R.K., 2014. Hydrothermal alteration associated with copper-gold mineralisation at Dhani Basri, Dausa district, Rajasthan: Use of Alteration Box plot—As an effective tool for determining the degree of alteration. J. Geol. Soc. India 84, 709–726.

Sharkhuu, L., 1980, Report on results of exploration and evaluation works with the scale of 1:50 000. 1:10 000 conducted in Kharmagtai copper ore field in 1979-1980: Report 3366, Geological Information Center, Mongolian Geological Survey, p. 159 (in Russian).

Sillitoe, R.H. and Perello, J. 2005, Andean copper province, tectonomagtic settings, deposit types, metallogeny, exploration and discovery: Economic Geology 100th Anniversary volume, p.845-890.

Sillitoe, R.H., 1993, Gold-rich porphyry copper deposits: Geological model and exploration implications: in Kirkham, R.V., Sinclair, W.D., Thorpe, R.I. and Duke, J. M., eds., Mineral Deposit modeling, Geological Association of Canada, Special paper 40, p. 465-478.

Sillitoe, R.H., 2000. Gold-rich porphyry deposits: descriptive and genetic models and their role in exploration and discovery: in Gold in 2000; reviews. Econ. Geol. v. 13, 315–345.

Sillitoe, R.H., 2010. Porphyry copper systems. Econ. Geol. 105, 3–41.

Sillitoe, R.H., Gappe, I.M., 1984. Philippine porphyry copper deposits: Geological setting and characteristics: CCOP technical. Publication 14, 89p.

Sorrentino, A., Chirico, R., Corrado, F., Laukamp, C., Di Martire, D., Mondillo, N., 2024. The application of PRISMA hyperspectral satellite imagery in the delineation of distinct hydrothermal alteration zones in the Chilean Andes: The Marimaca IOCG and the Río Blanco-Los Bronces Cu-Mo porphyry districts. Ore Geol. Rev. 167, 105998.

Theart, H.F.J, Ghavami-Riaba, R. Mouri, H and Graser P., 2011, Applying the box plot to the recognition of footwall alteration zones related to VMS deposits in a high-grade metamorphic terrain. South Africa, a lithogeochemical exploration application: Chemie der Erde – Geochemistry., v. 71, p. 143-154.

Titley, S.R., 1982. The style and progress of mineralisation and alteration in porphyry copper systems, American south-west, in Titley SR., Advances in the geology of porphyry copper deposits. In: Southwestern North Americas. University of Arizona press, pp. 93–116.

Vila, T., Sillitoe, R.H., 1991. Gold-rich porphyry systems in the Maricunga Belt. Northern Chile: Economic Geology 88, 1238–1260.

Wilkinson, J.J., Chang, Z., Cooke, D.R., Baker, M.J., Wilkinson, C.C., Inglis, S., Chen, H., Gemmell, J.B., 2015. The chlorite proximitor: A new tool for detecting porphyry ore deposits. J. Geochem. Explor. 152, 10–26.

Zhou, Y., Zhang, Z., Yang, J., Ge, Y., Cheng, Q., 2022. Machine learning and singularity analysis reveal zircon fertility and magmatic intensity: Implications for porphyry copper potential. Nat. Resour. Res. 31, 3061–3078.